(2)

PL-TR-92-2229

ADVANCED RETRIEVAL AND ANALYSIS OF SATELLITE DATA FOR NUMERICAL WEATHER PREDICTION

J.-F. Louis
R. G. Isaacs
T. Nehrkorn
R. N. Hoffman
C. Grassotti
M. Mickelson
J.-L. Moncet

Atmospheric and Environmental Research, Inc
840 Memorial Drive
Cambridge, MA 02139

10 November 1992

Final Report
23 February 1989-22 August 1992

PHILLIPS LABORATORY
Directorate of Geophysics
AIR FORCE MATERIEL COMMAND
HANSCOM AIR FORCE BASE, MA 01731-5000

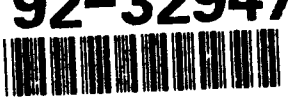

"This technical report has been reviewed and is approved for publication"

DONALD C. NORQUIST
Contract Manager

DONALD A. CHISHOLM, Chief
Atmospheric Prediction Branch

ROBERT A. McCLATCHEY
Division Director
Atmospheric Sciences Division

This report has been reviewed by the ESC Public Affairs Office (PA) and is releasable to the National Technical Information Service (NTIS).

Qualified requestors may obtain additional copies from the Defense Technical Information Center. All others should apply to the National Technical Information Service.

If your address has changed, or if you wish to be removed from the mailing list, or if the addressee is no longer employed by your organization, please notify PL/TSI, Hanscom AFB, MA 01731-5000. This will assist us in maintaining a current mailing list.

Do not return copies of this report unless contractual obligations or notices on a specific document requires that it be returned.

REPORT DOCUMENTATION PAGE

Form Approved
OMB No 0704-0188

1. AGENCY USE ONLY *(Leave blank)*	2. REPORT DATE	3. REPORT TYPE AND DATES COVERED
	11/10/92	Final Report 23 Feb. 1989 - 22 Aug.1992

4. TITLE AND SUBTITLE
Advanced Retrieval and Analysis of Satellite Data for Numerical Weather Prediction

5. FUNDING NUMBERS
Contract F19628-89-C-0044

PE 61102F
PR 2310
TA G7
WU EA

6. AUTHOR(S)
J.-F. Louis, R.G. Isaacs, T. Nehrkorn, R.N. Hoffman, C. Grassotti, M. Mickelson, J.-L. Moncet

7. PERFORMING ORGANIZATION NAME(S) AND ADDRESS(ES)
Atmospheric and Environmental Research, Inc.
840 Memorial Drive
Cambridge, MA 02139

8. PERFORMING ORGANIZATION REPORT NUMBER

9. SPONSORING/MONITORING AGENCY NAME(S) AND ADDRESS(ES)
Phillips Laboratory
Hanscom AFB, MA 01731-5000

Contract Manager: Donald Norquist/GPAP

10. SPONSORING/MONITORING AGENCY REPORT NUMBER
PL-TR-92-2229

11. SUPPLEMENTARY NOTES

12a. DISTRIBUTION/AVAILABILITY STATEMENT

Approved for public release; distribution unlimited.

12b. DISTRIBUTION CODE

13. ABSTRACT (Maximum 200 words)

This report documents the development and testing of an advanced geophysical parameter retrieval, analysis and prediction system for global numerical weather prediction. The additions and improvements to the existing data assimilation system at the Phillips Laboratory are the following: a new surface pressure analysis, modifications for high resolution analysis, an optimal retrieval of SSM/T data based on Bayesian estimation, use of precipitation data to improve the moisture and divergence analysis and as input to a diabatic nonlinear normal mode initialization. The system uses a version of the advanced physics global spectral model of PL.

The results of simulation tests show a significant improvement of the moisture analyses, especially in the tropics and Southern Hemisphere, and a smaller, but detectable improvement of the other variables, except in the stratosphere.

14. SUBJECT TERMS
Numerical weather prediction, data assimilation, OSSE, satellite retrieval, Bayesian estimation, diabatic normal mode initialization

15. NUMBER OF PAGES
80

16. PRICE CODE

17. SECURITY CLASSIFICATION OF REPORT	18. SECURITY CLASSIFICATION OF THIS PAGE	19. SECURITY CLASSIFICATION OF ABSTRACT	20. LIMITATION OF ABSTRACT
Unclassified	Unclassified	Unclassified	SAR

Table of Contents

List of Figures

List of Tables

1 Introduction

This report documents the development and testing of an advanced geophysical parameter retrieval, analysis and prediction system for global numerical weather prediction (NWP), performed under the Phillips Laboratory contract No. F19628-89-C-0044.

We called this system "CASCADE", because of the shape of the data flow diagram (see Figure 1) and because the work was designed to provide a series of incremental improvements to the system, each flowing into the next one. CASCADE is a step towards an advanced and nearly ideal analysis system for global NWP which, we feel, is attainable by the mid to late 1990's.

The modular design of CASCADE provided a basis for our work, which allowed us to make use of previous efforts and to concentrate on the aspects of the analysis system that are most important to the Air Force concerns and that may not be fully addressed by the operational meteorological centers. Modularity implies that the overall procedure can be easily reconfigured by replacing sub-procedures. CASCADE was developed step by step, incorporating:

- a variable resolution optimal interpolation scheme;

- an enhanced satellite data handling capability based on an optimal retrieval approach to process the DMSP sensor suite data including the SSM/T, SSM/T-2, and eventually SSM/I and OLS;

- algorithms to use satellite observed clouds to infer precipitation rates. The inferred precipitation rates are used to deduce latent heating profiles and to adjust the relative humidity field in convective regions;

- inclusion and testing of diabatic effects in the nonlinear normal mode initialization.

Four simulated data assimilation experiments were performed to test the various elements of the CASCADE system. These experiments were performed with data extracted from a "Nature run" provided by the European Centre for Medium-Range Weather Forecasts (ECMWF).

2 Background

Remote sensing from space and numerical weather prediction technology and practice have evolved significantly since their operational beginnings in the 1950s and 1960s. Inferences of atmospheric temperature and moisture, clouds, precipitation, winds, and surface properties can now be made from a variety of visible, infrared, and microwave satellite sensors. For global NWP it is primarily the retrieved temperature profile and wind data which have been used. The usefulness of other geophysical parameters for NWP is not yet well established and is largely untested, although a great many retrieval methods have been proposed or developed for a variety of potentially interesting parameters. The reason for this is twofold. On the one hand, these data are expected to have the most impact on mesoscale modeling, but mesoscale analysis systems are still relatively primitive. On the other hand, moisture variables - that is, specific humidity, clouds and precipitation - are retrievable and are potentially very useful, but are not easily assimilated by current methods. It is theoretically possible to retrieve specific humidity profiles by using methods analogous to those used to retrieve temperatures. However, results to date with available sensors have not been wholly satisfactory.

Other moisture parameters are somewhat easier to retrieve; for example, cloud cover may be obtained by a variety of techniques from imagery in visible and/or infrared spectral regions, and vertically integrated water vapor is well correlated with emissions at microwave frequencies, especially over the ocean. Unfortunately, these parameters are not readily assimilated by a global NWP model, and special methods are required. A variety of other meteorological parameters which may be used for NWP are retrievable. These include winds at the surface from microwave sensors and cloud drift winds aloft, as well as other surface properties, such as soil moisture, albedo, snow cover, temperature, and fluxes. The impact of current observing systems on global NWP is not large except in the southern hemisphere, where conventional data sources are limited. Increasing the accuracy and vertical resolution of the sensors and improving the retrieval and assimilation systems should lead to better forecasts. We believe that only a small part of the potential usefulness of satellite remote sensing for global NWP has been realized.

It is evident that improvements in NWP come from parallel progress in the forecast models, their resolution, numerical schemes and simulation of the physics, and in the analysis of the data that provide the initial conditions for the forecasts. Data analysis techniques have evolved considerably over the last few years, partly because of the introduction of new data types such as satellite data. The development of the optimal interpolation (OI) method, for example, was spurred by the fact that different data types have different error

characteristics. Nevertheless most, if not all, of the existing operational data analysis methods are still closely tied to the conventional type of data, namely radiosoundings, which provide profiles of the variables used by the NWP models, simultaneously at many points on the globe. Consequently much effort has been devoted in trying to make all data look like radiosoundings: the majority of all satellite data retrieval studies have been devoted to this goal.

It is being realized more and more, however, that trying to make all data look like radiosoundings may not be the best tactic. Indeed new types of data have fundamentally different characteristics. The most important differences are that they are asynoptic, nonlocal, indirect, and often incomplete (e.g. Doppler radar). Instead of being taken all at the same time like the synoptic data, they are taken more or less continuously or at random times. Remote sensing techniques sample a much larger volume of the atmosphere than do radiosondes, and the radiances that are measured are only indirectly related to the variables needed by the NWP models, through a convolution of the profiles by a complicated transfer function. In some cases (e.g. imagery data), very little NWP use has been made of vast quantities of data because of the difficulty of making them look like a radiosounding. The current thinking is that it would be preferable to use data directly, in the form and at the time they are taken. Different approaches have been taken, mainly using variational or Bayesian methods.

Another important problem of NWP is the analysis of moisture data. The humidity field tends to have a high variability at small scales, so that its determination from conventional data is rather poor. Up to now, not much use has been made of satellite data to help specify the moisture field. The result is a poor humidity analysis and, consequently, a poor humidity forecast. The first few hours of a forecast are usually characterized by a rapid re-adjustment of the moisture field to one compatible with the model thermodynamic structure. This process is accompanied by large variations in the precipitation rates and large changes in the diagnosed cloud cover. This is part of the so-called "spin-up" problem.

Related to this problem is the question of properly initializing or balancing the model mass and wind fields to avoid the development of large amplitude gravity waves. In this balance, one needs to take into account the effect of diabatic heating, especially the latent heat release. It is obvious that, with a poor moisture analysis, the diabatic heating cannot be computed properly. Conversely, if the latent heat release can be estimated (e.g. from imagery data), then a better moisture analysis may be made, more in balance with the thermodynamic field, thus reducing the spin-up problem.

The ultimate goal of data retrieval and analysis is to find a way of combining all the information that we have about the atmosphere and its processes in a

consistent manner and properly accounting for all aspects of the data. The methodology to achieve this goal will most likely be a four-dimensional (4-D) variational analysis of all available data, using an adjoint model to determine the gradient of the objective function (measuring the closeness between the model state and the measurements) with respect to the initial state. The data would include imagery, radiances and all conventional data. New data sources such as ground based lidar profilers with fine temporal resolution, space borne Doppler lidar wind profilers, etc. would be accommodated with ease. Within such a scheme, improvements to the model immediately yields improvements to the retrieval/analysis.

Most operational centers, including the National Meteorological Center (NMC), ECMWF and the French weather service, are working on this in a straightforward manner, developing the adjoint model methodology mentioned above. Although developing such a methodology in a few years was an effort that by far exceeded the resources available to us, we have kept this ultimate analysis in mind in our research effort. The work presented here on the development of CASCADE represents several steps toward this ultimate objective, making the best possible use of the work already completed by AER and Phillips Laboratory personnel, and keeping in focus the specific concerns of the US Air Force.

In the design of CASCADE we have followed some general principles which, we feel, are essential for the development of the ideal data assimilation method of the future. The main points are the following:

(1) Use of all available data. Although using all data is obviously desirable, we have seen that, for various reasons, many types of data are currently not used at all. CASCADE does not achieve this requirement either, but it uses more fully the data from the DMSP suite of instruments, as well as imagery data (or RTNEPH data as a surrogate for imagery).

(2) Use of remotely sensed physical forcing mechanisms such as latent heating. For example, since the effect of latent heat release is important in intense storms, it is natural to consider using observed precipitation rates to force the model by an externally specified heating function during an assimilation period. In CASCADE, a first step is taken by using estimates of latent heating that can be derived from remotely sensed data in the nonlinear normal mode initialization.

(3) Direct use of remotely sensed data through a variational analysis rather than by a retrieval method. Such a procedure avoids the introduction of errors by the retrieval technique and allows optimal use (in a Bayesian sense) of the data. This has been the main thrust of our effort.

While CASCADE is a step towards an ideal data assimilation system, it still falls short in a number of ways. The most important principles that CASCADE does not follow are:

(1) Using data continuously without time lags. The conventional practice of batching data into 6 h increments is still followed by CASCADE. This is reasonable as long as only the largest scales are under consideration. With increasingly fine mesh models and high resolution observations, smaller scales will become more important, and a 6 hour data increment will blur the observational picture.

(2) Reducing the need for normal mode initialization. Normal mode initialization procedures are reasonable approaches when certain assumptions are met, but these assumptions are less valid in the tropics where the Rossby number is not small, and in the boundary layer where the effect of friction is strong. Nevertheless, the design of CASCADE still requires the use of an initialization.

These two unmet requirements can be resolved only with a fully quadridimensional data assimilation system. For the time being, CASCADE remains a tridimensional scheme, doing data analysis intermittently in six hour intervals.

3 Experimental Design

3.1 The design of CASCADE

CASCADE is described in block form by Fig. 1. This is a data flow description. The arrows in the figure represent data being transferred; black when the data are model states (i.e. a complete description of the model atmosphere: normally, u, v, Z, p^*, rh), white when the data are observations and gray when the data are auxiliary variables that are derived either from the model variables or the observations. Each step of CASCADE adds new (i.e. independent) information. Wherever possible, the background field and observations are combined to minimize the probable analysis error.

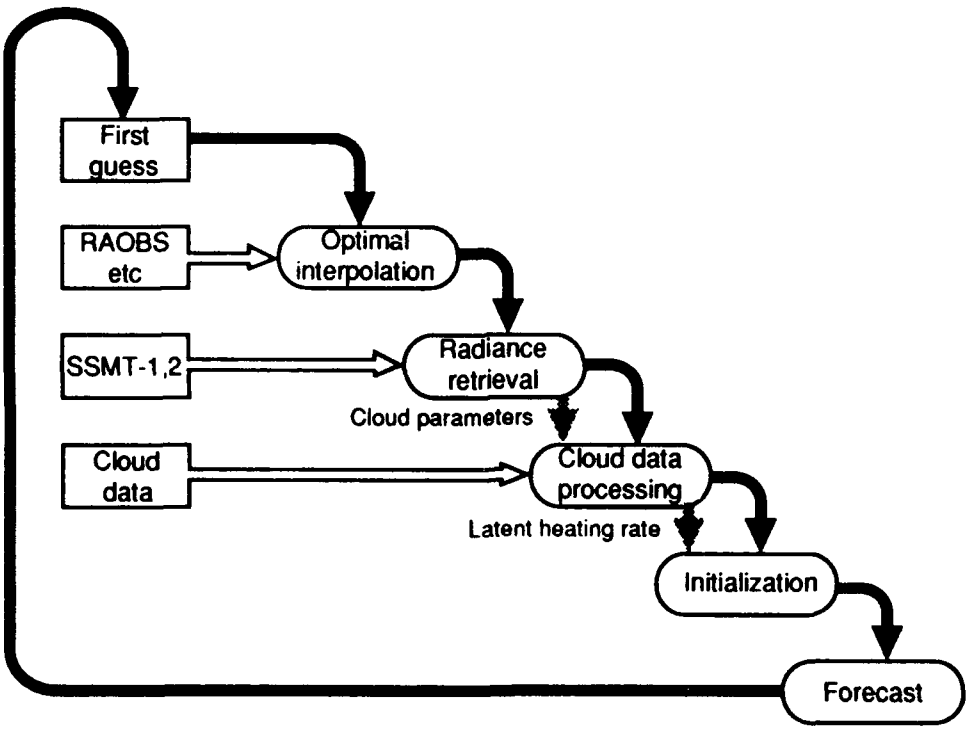

Figure 1: Data flow diagram for CASCADE. The black arrows represent the model variables, the white arrows the data, and the gray arrows auxiliary variables that are computed by the system.

CASCADE starts with a standard optimal interpolation analysis of the conventional data and other usual data including aircraft data, cloud drift winds and operational NOAA TOVS satellite temperature soundings. At the next step (radiance retrieval), data from the SSM/T-1 and SSM/T-2 are used to improve the analysis of temperature and moisture. Changes in the extratropical temperature fields are reflected in the wind analysis by geostrophy. Horizontal consistency is insured by an appropriate filter. After this step cloud information is used to refine the moisture analysis. It is also

used to determine latent heating rates which become a constraint in the initialization that follows.

CASCADE differs from an ideal scheme in two important ways. First of all, as has already been mentioned, it is an intermittent scheme, with all data grouped in batches and analyzed together every 6 hours. Secondly, each retrieval is split into a vertical (retrieval proper) and horizontal (smoothing) component. In an ideal system the analysis would be a continuous process, and the vertical and horizontal components of the retrievals would be combined. Note that we avoid the problem of retrieval - first guess correlations by processing the different data in series instead of in parallel.

CASCADE was developed in a series of steps, each one adding a new module. The baseline version consisted of modules that were, for the most part, already available, although we had to make fairly substantial improvements to the existing OI to include a surface pressure analysis and to use a higher resolution model.

In the following sections we present the various modules making up CASCADE. In each section we first briefly describe what was already available to build up version 1.0, then we detail improvements that were made.

3.1.1 Optimal interpolation

The starting point for CASCADE was the ASAP optimal interpolation scheme that has been developed at AFGL (now the Phillips Laboratory). The ASAP OI was developed by SASC for AFGL/LYP and is documented in a series of reports by Norquist and others (Halberstam *et al.*, 1984; Norquist, 1982; Norquist, 1983; Norquist, 1984; Norquist, 1986). The ASAP OI is based on the NMC assimilation system (Bergman, 1979; McPherson *et al.*, 1979), but was thoroughly redesigned and recoded by SASC personnel. It is a multivariate analysis of height and wind components and a univariate analysis of relative humidity, both in model sigma layers.

Data used by the height-wind analysis include Type 1 observations (radiosondes, pibals, etc.), Type 2 observations (aircraft), Type 4 observations (satellite-retrieved temperatures or thicknesses) and Type 6 observations (cloud drift winds (CDWs)). The Type 3 surface observations are not used at all. The moisture analysis, in the original ASAP, uses only Type 1 data. The CDW data (Type 6 data) are combined (i.e., locally averaged) into super-obs. There are two principal reasons for doing this: first, to limit the total number of observations, so that computer memory restrictions are not exceeded, and second, the CDW errors are strongly related horizontally because the main error source is due to height assignment (McPherson, 1984).

The version of the OI used at the start of the project included

1) a strict decoupling of height and wind analysis in the equatorial belt,

2) the simultaneous solution for heights and winds so increments are geostrophically balanced (normal equations are now solved using LINPAK routines),
3) an underground analysis of heights and winds, to assure smooth extrapolation of height analysis increments to the surface,
4) correct specification of the right hand side of the normal equations, and
5) a more efficient and accurate method of converting satellite thicknesses to level heights.

Three sets of modifications were made to the OI code to produce the baseline version: implementation of variable resolution, introduction of a surface pressure analysis, and modified data selection for the lowest layers.

3.1.1.1 *Variable resolution code changes*

A series of changes were made to the analysis codes (ASAP and MASAP for moisture) and their associated pre- and postprocessors to allow for variable resolution.

The changes to the analysis codes were made as a series of small changes, which enabled us to reproduce the results of the initial code with small errors, the source of which we clearly identified. Significant changes have been reflected in the new documentation for ASAP, which was published as a scientific report (Hoffman *et al.*, 1988). The main changes are the following:

All common blocks are now incorporated in the code by "include" statements and are the same whenever they are used.

The constants for LOWTMP (the Flattery algorithm) are calculated once at the start of ASAP, since these constants depend on the vertical structure.

The first guess error growth rates are stored at mandatory levels and interpolated to the sigma structure instead of being hard-wired for a particular model structure.

The code for the 3DNeph and surface weather options (used by Norquist, 1988) has been deleted.

The code is now strictly standard FORTRAN.

Modifications for MASAP paralleled those for ASAP. The largest differences during this series of modifications are due to the calculation of the LOWTMP constants to full machine precision instead of specifying them on a DATA statement to 9 or 10 digits, and to the change in the error growth rate computation, which produced differences detectable at the $O(10^{-3}$ g/kg) level.

The pre- and postprocessors (PPPs) were completely redesigned, in a modular fashion. Since the global spectral model (GSM) PPPs already exist in variable resolution format, we only implemented our design for the PPPs for the OI. Many of the subroutines needed to affect the implementation for the GSM are

now available, and the two sets of PPPs could be unified at some later date. This has been done for the GSM postprocessor. The subroutines were tested extensively.

Three new main modules were coded and tested:

- Spectral to grid point (OISTG): Reads in spectral coefficient data set and writes out the grid point first guess files.

- Grid point to spectral (OIGTS): Reads the analysis grid point files, updates the pressure field and outputs the spectral coefficient analysis file.

- Spectral filter for estimated analysis error (PREAES). Reformats height and relative humidity estimated analysis errors.

3.1.1.2 Surface pressure analysis

Early in the project we decided to re-examine the question of how to arrive at sigma-layer temperature increments from an analysis of geopotential height. Results from our previous contracts (Hoffman *et al.*, 1990; Louis *et al.*, 1989) had indicated that the lack of a surface pressure analysis, the neglect of surface data, and the consequent anchoring of the satellite thicknesses to the first guess surface pressure severely limited the applicability of the results from our OSEs and OSSEs. We had been especially concerned about the relatively large errors of our analyses. In particular the height analyses did not fit the RAOBs closely enough. In the Northern Hemisphere, where the RAOBs are close together, the lack of fit should be about the size of the RAOB observation error standard deviation (OESD). However the RAOB OESD at 500 hPa is only about 12 m, while our typical RAOB analysis difference was 40 m.

As a first step toward addressing this problem, we removed the anchoring of radiosonde heights to the first guess surface pressure and conducted a test assimilation for 24 hours. Results indicated a better fit to the 500 hPa geopotential, but rapidly growing, large errors at 1000 hPa as a result. It became clear, then, that an analysis of surface pressure was required.

A new surface pressure update similar to that used by the ECMWF was instituted. The new formulation uses the lowest and underground layer height increments to estimate the height increment at $\sigma = 1$, which is then converted hydrostatically to a pressure increment. With these corrections the overall impact is a significant improvement. For example, Fig. 2 shows the impact on the 500 hPa height analysis.

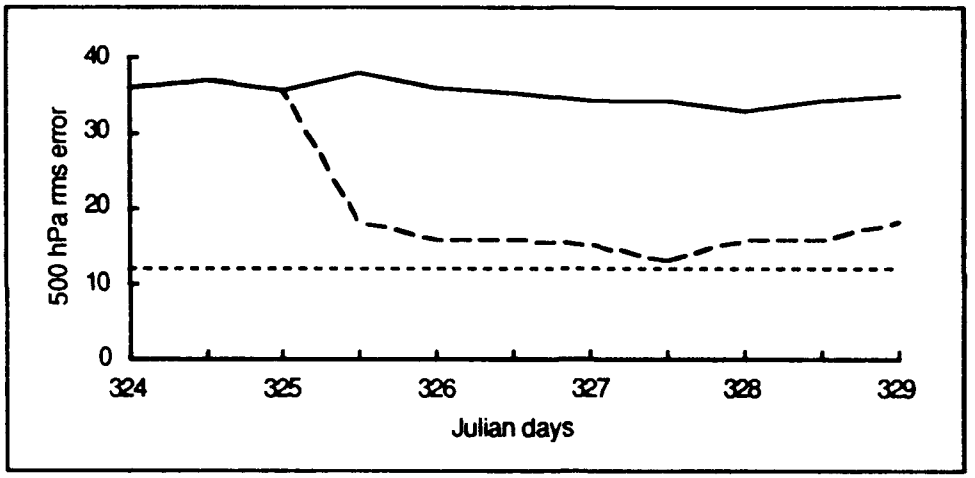

Figure 2: Impact of improved surface pressure analysis on 500 hPa rms analysis error for the Northern Hemisphere extratropics. The surface pressure experiment (dashed line) starts on Julian day 325, from a state identical to the control experiment (solid). The RAOB observation error standard deviation (dotted) is shown for reference.

3.1.1.3 Data selection for bottom layers

Because of the need to resolve the boundary layer structure in the forecast model, the bottom layers of the model (and the analysis) are very thin. This can lead to problems in the conversion of the height increments to temperature increments: if different data are selected for adjacent layers, the height increments will differ by an amount that can imply an unreasonably large temperature increment. To avoid this problem, we added an option to the OI to enforce identical data selection for the lowest layers (plus the underground layer). This was done by temporarily resetting the pressure of the sigma layer to a constant value for all these layers during data selection, and subsequently restoring it to its proper value when the actual correlations for the analysis weights are computed. In our implementation, this data selection was enforced for the lowest 4 layers.

3.1.2 Radiance retrieval

A major disadvantage of the operational statistical retrieval is that, in regions with sufficient conventional data, the NWP model forecast fields themselves may be more accurate than the satellite retrievals for initialization purposes. Therefore, assimilation of the satellite data would naturally tend to degrade the quality of forecasts rather than to improve them. This property of the statistical retrieval is due to its dependence on precomputed statistics which imply a first guess which is essentially climatology. Isaacs' unified retrieval (Isaacs, 1987) sought to circumvent this problem by using the statistical

retrieval only as a first guess. A physical retrieval step was then employed to reconcile the retrieved state of the atmosphere with the radiance data itself.

Eyre (1988) points out several other problems of the operational retrieval schemes in addition to this implied first guess dependence. These include errors from the cloud clearing algorithms and the manner in which the satellite data are treated in the assimilation process. For CASCADE, we have used Eyre's optimal retrieval scheme, which operates directly on the radiance data, thereby bypassing the error generating preprocessing and cloud clearing steps in the conventional approach. His method may be considered either as a retrieval scheme which uses the forecast model to provide first guesses to the desired state variables and then provides retrievals which are consistent with the model, or alternatively, and equivalently, as a module within the analysis scheme which performs the analysis of the satellite data in the vertical.

The background or first guess field for the optimal retrieval of Eyre is the forecast model itself. In our implementation, the background field is the analysis produced by the OI. The mathematics of the retrieval requires the evaluation of the forward problem and its derivatives with respect to the atmospheric state vector elements. The optimal retrieval uses information related to both the data and the background or forecast first guess field to constrain the inversion.

The optimal retrieval is characterized mathematically in the following way: The retrieval seeks to find the most probable atmospheric state vector, x, given a set of measurements, i.e. the satellite radiance data, y^m. By Bayes' theorem this conditional probability, $P(x|y^m)$, is proportional to the product: $P(y^m|x) \cdot P(x)$. The first factor is the probability of making the measurements given the state of the atmosphere, while the second is the probability of the atmosphere being in that state. The former can be related to the covariance matrix of the measurement error for the satellite data, while the latter can be related to the forecast model error covariance assuming that the NWP model provides the first guess. It is assumed that both error sources have Gaussian error statistics. The most probable atmospheric state given the measurements and the forecast first guess then involve these error covariance matrices and, in addition, the derivative of the forward problem with respect to the state vectors.

The optimal retrieval scheme treats the nonlinearities of the retrieval problem such as that introduced by cloud clearing through Newtonian iteration. The residuals, i.e. the differences between the actual and calculated radiances for a given guess of the state vector, provide information on the convergence properties of the retrieval. Eyre derives a retrieval error covariance matrix, S, which can be used to address the problem of assigning weights to the retrievals within the horizontal analysis. The problem of correlation between errors in the first guess (i.e. the forecast) and the

retrievals is also addressed. A detailed description of the method can be found in Appendix B.

We have employed the optimal retrieval scheme with the DMSP microwave sensor suite of instruments (Falcone and Isaacs, 1987). State vector elements which can be treated by the optimal retrieval include temperature and moisture profiles, surface temperature, and cloud parameters. SSM/I is particularly useful for the quality control, providing a precipitation flag. Potentially, rain rate, or latent heating rate information from SSM/I could be provided to the initialization. A number of cloud parameters are potentially retrievable from the DMSP sensors. In this work we have limited the retrievals to temperature and moisture profiles.

In the configuration provided to us by J. Eyre (TOVCFG), the scheme was set up for application to TIROS Operational Sounder (TOVS) data and included surface microwave emissivity, cloud-top pressure and effective cloud amount among the retrieved parameters. The algorithm used a forecast profile as a background constraint and as a first guess for temperature and humidity parameters. The associated error covariance matrix, C, were constructed from a set of forecast error statistics supplied by the Forecasting Research Branch of the U. K. Meteorological Office.

The TOVCFG program was implemented on the Alliant computer at AER and was subsequently modified so it could be used for simulation runs. By being able to directly compare the retrieved parameters with the "true" values used to generate a set of simulated TOVS radiances, we were able to evaluate the performance of the retrieval algorithm and at the same time check for potential coding errors which might have occurred in the process of transferring the code to the Alliant system.

As part of our simulation tool, we developed a module that first does the vertical interpolation and extrapolation of a selected forecast profile from the nature run to the 40 standard National Environmental, Satellite, and Data Service (NESDIS) levels used by the radiative transfer algorithm. A "true" profile x^t is then constructed by perturbing the resulting background profile x^b as follows:

$$x^t = x^b + \sum_i \varepsilon_i \sqrt{\lambda_i} v_i \qquad (1)$$

where λ_i and v_i are the eigenvalues and associated eigenvectors of the forecast error covariance matrix and ε_i are samples of a Gaussian population with zero mean and unit variance. In this way, the perturbation has the same covariance as the forecast errors. Both "true" profile and background profile are checked and if necessary, corrected for supersaturation. Finally, a vector of simulated TOVS radiances is obtained by applying the forward model to the

"true" profile and by adding random Gaussian noise of covariance E to the calculated radiances.

Figures 3 and 4 show examples of simulated retrievals for a clear-sky case and a cloudy case, respectively. The same temperature and humidity profiles have been used in both experiments.

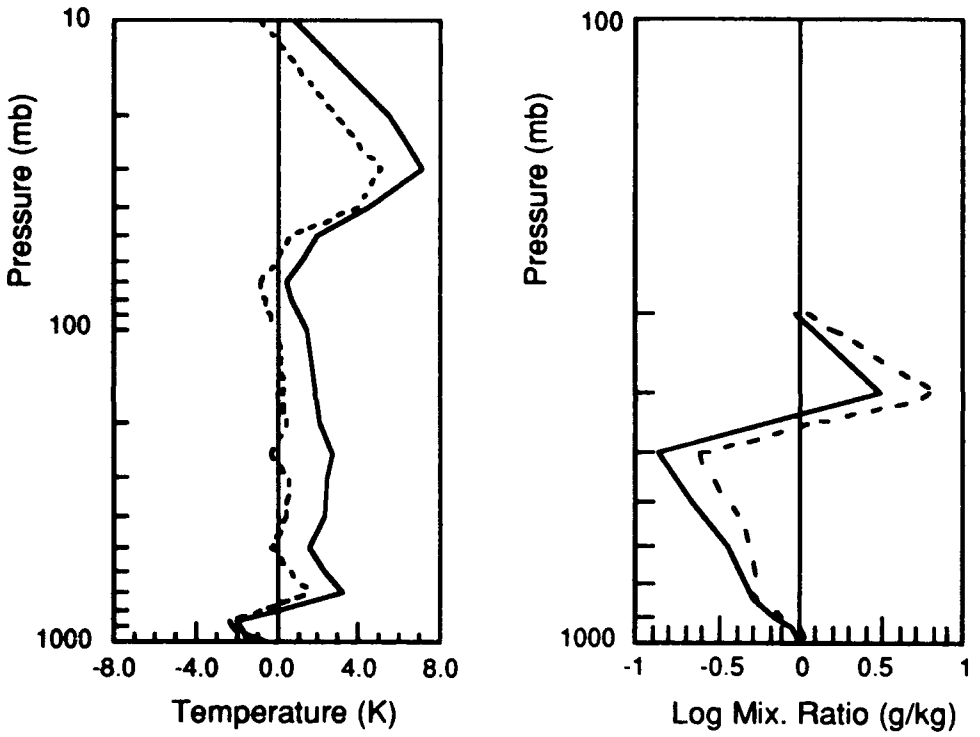

Figure 3 Example of retrieval for a clear case. The solid lines are the first guess errors of temperature (left) and logarithm of specific humidity (right). The dashed lines are the corresponding retrieval errors

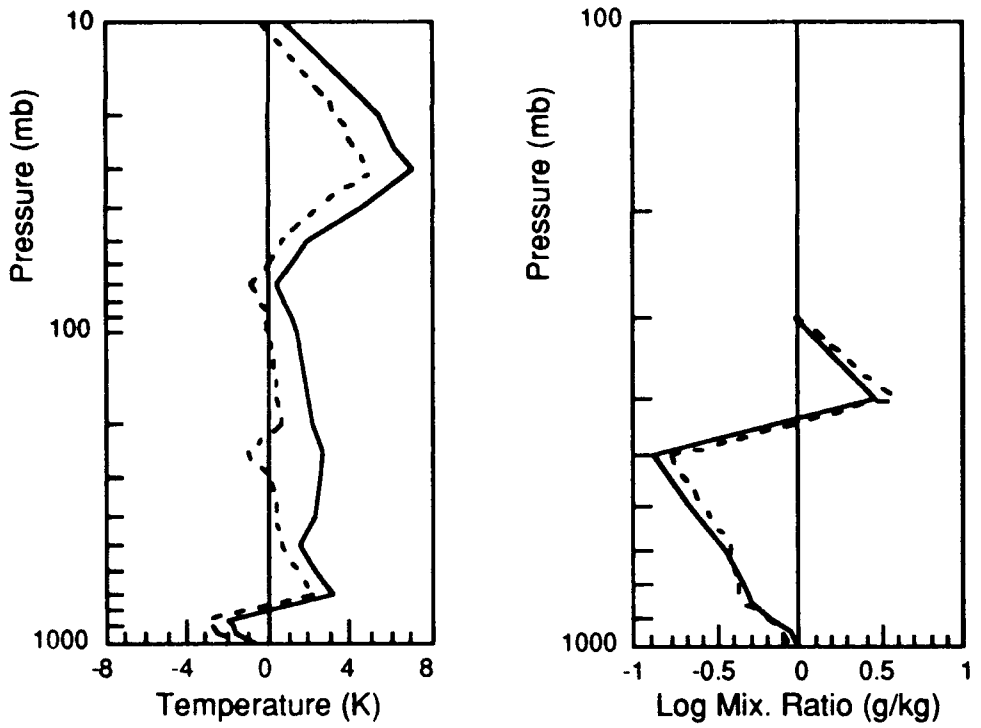

Figure 4 : Same as Fig. 3, but for a cloudy case.

3.1.3 Horizontal smoothing algorithm

A horizontal smoothing algorithm is used within CASCADE to distribute retrievals from observing locations to grid points in the horizontal. We have received and tested the recursive filter by Hayden and Purser (1988) for this purpose. This filter is a fast algorithm that is essentially equivalent to a Barnes analysis. We generalized the software to allow the use of variable grid spacing (such as latitude-longitude grids), and we developed guidelines for choosing the adjustable parameters of this filter based on the work of Seaman (1989). Seaman derived optimal values for the Gaussian length scale of the Barnes scheme based on the statistical properties of the background field and the observations. We did not, however, implement this part of CASCADE in the simulation experiments described here.

3.1.4 Cloud data processing

The purpose of this module is to use cloud data, such as from the RTNEPH or other cloud analysis system, to refine the moisture analysis. It is also used to provide latent heating rates for the subsequent initialization step. Both Molinari (1982) and Fiorino and Warner (1981) obtained improved forecasts of intensity (relative to control experiments) when specified latent heating was used during a 12 h assimilation prior to the forecast. In addition,

Molinari obtained improved storm track forecasts and Fiorino and Warner obtained improved precipitation forecasts.

Satellite-derived cloud parameters have great potential in this regard. Several authors (see reviews by Martin and Scherer, 1973, and Atlas and Thiele, 1981) have shown that precipitation rates can be specified from satellite data, and Julian (1984) has proposed that the vertical profile of the divergence (or, equivalently, vertical velocity) can be related to cloud top equivalent black body temperature (EBBT) in the tropics. Therefore, it should be possible to specify latent heating rates from observed cloud characteristics. In our simulation experiments we simply used the precipitation information existing in the ECMWF nature run as a proxy for cloud data.

A possible extension of this work would be to use cloudiness data in another retrieval/analysis step in the framework of a series of successive optimal analyses/retrievals. The formalism of Eyre (1988) for radiances could be applied here as well, with the forward problem consisting of the computation of cloud value from the analysis variables.

3.1.5 Initialization

The normal mode initialization (NMI) is a part of the forecasting system which adjusts the initial data in such a way that undesirable gravity waves do not grow in the forecast. The ASAP NMI is based on the NMC NMI, which is described by Ballish (1980).

If diabatic heating effects are not included, NMI tends to suppress the Hadley circulation. A number of devices to improve the initialized tropical fields within the context of adiabatic NMI have been suggested (Puri, 1983; Puri *et al.*, 1982), but including diabatic processes is desirable, because the latent heat of convection is so clearly important in the balance of the tropical motions (Puri, 1985). It is not surprising, therefore, that some of Rasch's (1985b) findings suggest that a good humidity analysis is vital to diabatic nonlinear NMI. Unfortunately, diabatic nonlinear NMI has been found to have poor convergence characteristics and may actually increase the amplitudes of the high frequency noise at the start of the forecast (Rasch, 1985a).

An additional approach to improving the diabatic nonlinear NMI convergence characteristics is to hold the latent heating fixed. Mohanty et al. (1986), in their study of the impact of diabatic heating on nonlinear NMI, obtained their best results using "observed" diabatic heating. These were "observed" by calculating the residual of the thermodynamic equation averaged over 24 h from ECMWF analyses. Similar conclusions were drawn by Puri (1985).

In the simulation experiments reported here, observed precipitation rates were used in a moist initialization procedure which consisted of an

initialization step and a forecast modification of the first guess forecast. The forecast modification consisted of a rescaling of the predicted convective heating (and precipitation) by the ratio of observed to predicted convective precipitation for all grid points in the tropics with non zero predicted convective rain. The factor was not allowed to exceed the maximum value of 10. The three components of the initialization step consisted of a diabatic NMI, a separate divergence adjustment step in which vertical profiles of horizontal divergence were adjusted based on observed precipitation rates, and a temperature and moisture adjustment step designed to bring predicted convective precipitation rates in closer agreements with observations. The formulation of this procedure is described in full detail in Appendix C.

3.2 Experimental set-up

All the experiments performed in this project were done in simulation mode. The experimental set-up was the same for all the tests, and was similar to the one used for observing system simulation experiments (OSSEs) in our previous work (Grassotti *et al.*, 1989; Hoffman *et al.*, 1990).

The data is extracted from a nature run, which is an extended simulation performed with a different model. From an initial state given by the nature run we first perform what we call a spin-up experiment. It consists of a 4 day forecast, which gives a simulated atmospheric state with errors greater than the expected analysis errors, followed by 3 days of data assimilation, with the baseline system. This provides the initial state for all the experiments. Each experiment consists of 7 days of data assimilation, and 4 day forecasts starting from days 3, 5 and 7 of the assimilation period. A schematic overview of this experimental setup is shown in Fig. 5. Since the "truth" is known, as given by the nature run, we can compute analysis and forecast errors, by subtracting the nature run from the analyzed and forecast fields.

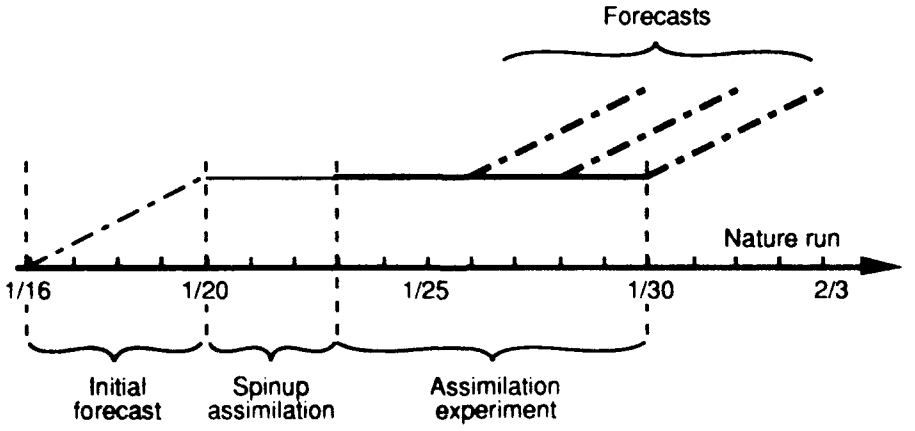

Fig. 5: Schematic showing the sequence of spinup forecast, spinup assimilation, 7-day assimilation, and 4-day forecasts from day 3, 5, and 7.

3.2.1 The Nature run

The nature run used in these experiments is an extended simulation created by ECMWF. Its horizontal resolution corresponds to a triangular 106 truncation in spectral space, and it has 19 levels in the vertical (however, the data available to us contained data on 14 mandatory pressure levels between 1000 hPa and 10 hPa). The simulation starts from 00GMT, 16 January 1979. The tapes containing the data were provided to us by NASA/GLA.

In addition to all the prognostic variables (temperature, winds, specific humidity, surface pressure, surface temperature and moisture, and snow amount), the tapes contain a number of diagnostic fields such as precipitation and surface fluxes. The data are stored every 3 hours for 31 days[1].

3.2.2 The simulated observations

The simulated observations were generated by adding appropriate errors to "perfect observations" extracted from the nature run. These perfect observations are simply the value of the nature run interpolated to the position of the actual observations available during the period corresponding to the nature run[2]. We did not interpolate in time. Instead, we assigned the observations to the nearest synoptic time. We give here a short summary of the procedures for adding errors, which are described in detail in Appendices A and B.

Errors of representativity were added as random, uncorrelated errors. The error magnitudes were determined from the observed spectra reported in Nastrom and Gage (Nastrom and Gage, 1985; Nastrom *et al.*, 1984). No attempt was made to compensate for the smoothing of the highest resolved wavenumbers in the ECMWF nature run.

We added random errors to perfect observations of types 1 (Raobs), type 2 (aircraft obs), and type 6 (satellite track winds), with vertical correlation where appropriate. For type 4 (satellite retrievals from TOVS), we performed a full simulation rather than add errors to the perfect observations. The error adding software additionally sorted the observations by latitude and, in the case of the satellite track winds, superobservations were formed.

We used a different method to simulate the optimal retrieval of SSM/T data. The SSM retrievals could be estimated in a straightforward fashion by simulating each step of the Eyre procedure. This would involve computing

---

[1]We received only the first 18 days of data.

[2]The perfect observations were supplied to us by STC .

radiances from the nature data to simulate the observations, computing radiances from the first guess (the OI analysis in our case) and modifying it iteratively to find the most probable profile compatible with the first guess and the observations. More details can be found in Appendix B.

An accelerated method for the simulation of retrievals of profiles and other geophysical parameters from microwave sounders has been used, based on Rodgers' (1990) linear error analysis. The approach takes advantage of the fact that the target profiles, taken from the nature run in the simulation studies, are known. It is assumed that the solution of the non-linear retrieval algorithm converges towards a point close to the target profile in the "measurement space" and that the magnitude of the combined radiometric and forward model errors remains reasonably small, so that their effect can be accounted for by applying a linear perturbation to the target profile. Under these assumptions, the solution profile can be expressed as a linear combination of the target and first guess profiles and the radiometric noise. The weights are derived from the error covariance matrices.

The amount of computation required to simulate a retrieved profile with this approach is roughly equivalent to one step of the classical Newton iteration procedure used in non-linear retrieval algorithms. Computational savings are the results of skipping the successive iteration steps normally needed to bring the solution to convergence.

An assessment of the validity of this approach was made based on comparisons between the solutions obtained with the accelerated method and the ones obtained by applying Eyre's retrieval algorithm. The Eyre code has been modified to perform retrievals of temperature and moisture profiles from simulated SSM/I , T and T-2 microwave data. Results of the comparison, obtained with realistic noise data, indicated that the retrieval solution can be estimated using the fast algorithm with an accuracy better than 1%.

3.2.3 The baseline data assimilation system

The baseline data assimilation system consists of the GSM, ASAP OI, and an adiabatic NMI. The version of the GSM used in our study was determined from the results of several test forecasts. It is the Phillips Laboratory GSM with advanced physics (see next section). We used it in a configuration with a rhomboidal 40 truncation, and 18 layers (σ interface values are 1.0, .990, .973, .948, .893, .820, .735, .642, .546, .45, .40, .35, .30, .25, .20, .15, .10, .05, and 0). A time step of 15 minutes was used; the diffusion coefficient for the horizontal diffusion was set at 2.55×10^{15} m^4/s.

The ASAP OI system, modified as described above, performed the analysis on the model σ layers on a 81x82 Gaussian grid.

The adiabatic NMI was identical to that used in our earlier work. It is a standard 2-iteration Machenhauer scheme, using the lowest 4 internal modes with a frequency cutoff of 48 hours.

3.2.4 The spinup experiment

We made several spin-up forecasts, with different versions of the GSM. We settled on a version that uses a general truncation version of the hydrodynamics code, and vectorized versions of the physics packages (Nehrkorn *et al.*, 1991). Its physics package consists of the Oregon State University planetary boundary layer package (Mahrt *et al.*, 1987), the University of Illinois Kuo convection (Soong *et al.*, 1985), and a modification of the University of Utah radiation package (Liou *et al.*, 1984), developed by the PL and the AER climate group. It includes a number of enhancements to the radiation code itself and uses the Slingo (1987) scheme for cloud diagnosis, tuned to give reasonable cloud cover and cloud forcing climatologies.

Following the spinup forecast, a three-day assimilation with the baseline data assimilation system was performed. The baseline system included the GSM, the OI, and an adiabatic NMI, as described above.

3.3 The CONTROL OSSE

This OSSE is a simple 7-day continuation of the spinup assimilation experiment, with 4-day forecasts generated from the initialized analyses at days 3, 5, and 7. It was designed to document the performance of the baseline data assimilation system, and to provide a benchmark for comparison with the other OSSEs.

3.4 The SSMTRAD OSSE

This OSSE differs from the CONTROL OSSE only in that the radiance retrieval step of SSM/T radiances was included in the data assimilation scheme. It was designed to test the radiance retrieval technique, and to determine the impact of the SSM/T data. The details of the radiance retrieval implementation in our OSSE, and results from these simulated retrievals, are discussed in detail in Appendix B; results of the OSSE itself are discussed in section 4.2.

3.5 The MOIST INIT OSSE

The MOIST INIT OSSE is identical to CONTROL, except that the adiabatic NMI is replaced by a moist initialization procedure. The moist initialization was designed to explore and test methods of using observed precipitation rates in the CASCADE data assimilation scheme. In this exploratory study, no errors were added to the nature run precipitation. The impacts thus represent an upper limit for the techniques employed here. The methods were

implemented as an initialization step and a modification of the first guess forecast.

The forecast modification was motivated by the finding that using observed diabatic heating within the diabatic NMI lead to improved results. It stands to reason, then, that additional benefit can be gained by forcing the forecast model used to provide the first guess for the next analysis cycle with observed diabatic heating rates. We implemented this as a rescaling of the predicted convective heating (and precipitation), at each time step and at all grid points in the tropics with non zero predicted convective rain, by the ratio of observed to predicted convective precipitation. The factor was not allowed to exceed the maximum value of 10. The observed precipitation was the nature run total precipitation rate for the 6-hour period centered at the inital time (the same observed precipitation rate was used for the forecast modification and the moist initialization). In a real data experiment, observed precipitation rates would have to be inferred from mostly remote sensing measurements.

The initialization step followed all other analysis/retrieval steps of CASCADE. The three components of the initialization step consisted of a diabatic NMI (using tendencies computed from the GSM with full physics, with diabatic heating in the tropics rescaled as in the first guess forecast, and a 2-iteration Machenhauer NMI), a separate divergence adjustment step in which vertical profiles of horizontal divergence were adjusted based on observed precipitation rates, and a temperature and moisture adjustment step designed to bring predicted convective precipitation rates in closer agreements with observations. The three components were combined into a multistep procedure, as follows:

step 1: diabatic NMI
step 2: divergence adjustment
step 3: temperature and moisture adjustment
step 4: diabatic NMI
step 5: temperature and moisture adjustment

The development and testing of the initialization procedure are described in detail in Appendix C; results of the OSSE itself are discussed in section 4.2.

3.6 The CASCADE OSSE

The CASCADE observing system simulation experiment combines all the parts tested separately by the previous two OSSEs: use of the optimal retrieval of SSM/T data and use of precipitation data both for modifying the moisture and divergence fields, and for moist initialization.

4 Results of Observing System Simulation Experiments

4.1 Performance of baseline assimilation system

The 500 hPa rms errors of geopotential height (z) displayed in Fig. 6 give a good illustration of the spinup phase of our OSSEs. During the initial spinup forecast, global errors grow from approximately 10 m 12 hours into the forecast to approximately 40 m after 4 days. The spinup assimilation, which used the endpoint of the 4-day forecast as its starting point, reduces the error to approximately 28 m globally. Analysis[3] errors have stabilized by the end of the 3-day assimilation, indicating the success of the spinup procedure. In the Northern Hemisphere extratropics, where data density and quality is highest, the error reduction is quicker and final rms errors are on the order of 18 m; in contrast, the Southern Hemisphere shows little reduction at all because of the lack of RAOB data (statistics over Australia, not shown here, show a reduction in error that is in agreement with the better coverage over that region).

The analysis errors in the CONTROL OSSE (which is the continuation of the spinup assimilation for another 7 days) show little variation with time, aside from a slight increase in Southern Hemisphere errors in the second half of the week.

Time series of 700 hPa relative humidity (*rh*) and the 700 hPa and 300 hPa horizontal wind rms errors (Fig. 7-9) show qualitatively similar behavior for CONTROL, except that the error reduction is clearly evident only in the Northern Hemisphere extratropics. In the tropics and the Southern Hemisphere, the CONTROL assimilation merely succeeds in halting the growth of the errors.

Vertical profiles of the analysis errors, averaged over the last 5 days of the assimilation, provide another view of the analysis system performance. The geopotential errors shown in Fig. 10 are nearly constant with height below the tropopause with values between 20 m (Northern Hemisphere) and 50 m (Southern Hemisphere). They quickly increase with height in the stratosphere; this increase is at least partially due to errors introduced in the interpolation from σ layers to mandatory pressure levels. The temperature errors (Fig. 11) show a similar behavior as the height errors, except for comparatively large values at 1000 hPa and 850 hPa. The latter are most likely due to different treatment of underground values between our and the ECMWF postprocessor.

---

[3]In this and all following statistics, analysis refers to the initialized analysis.

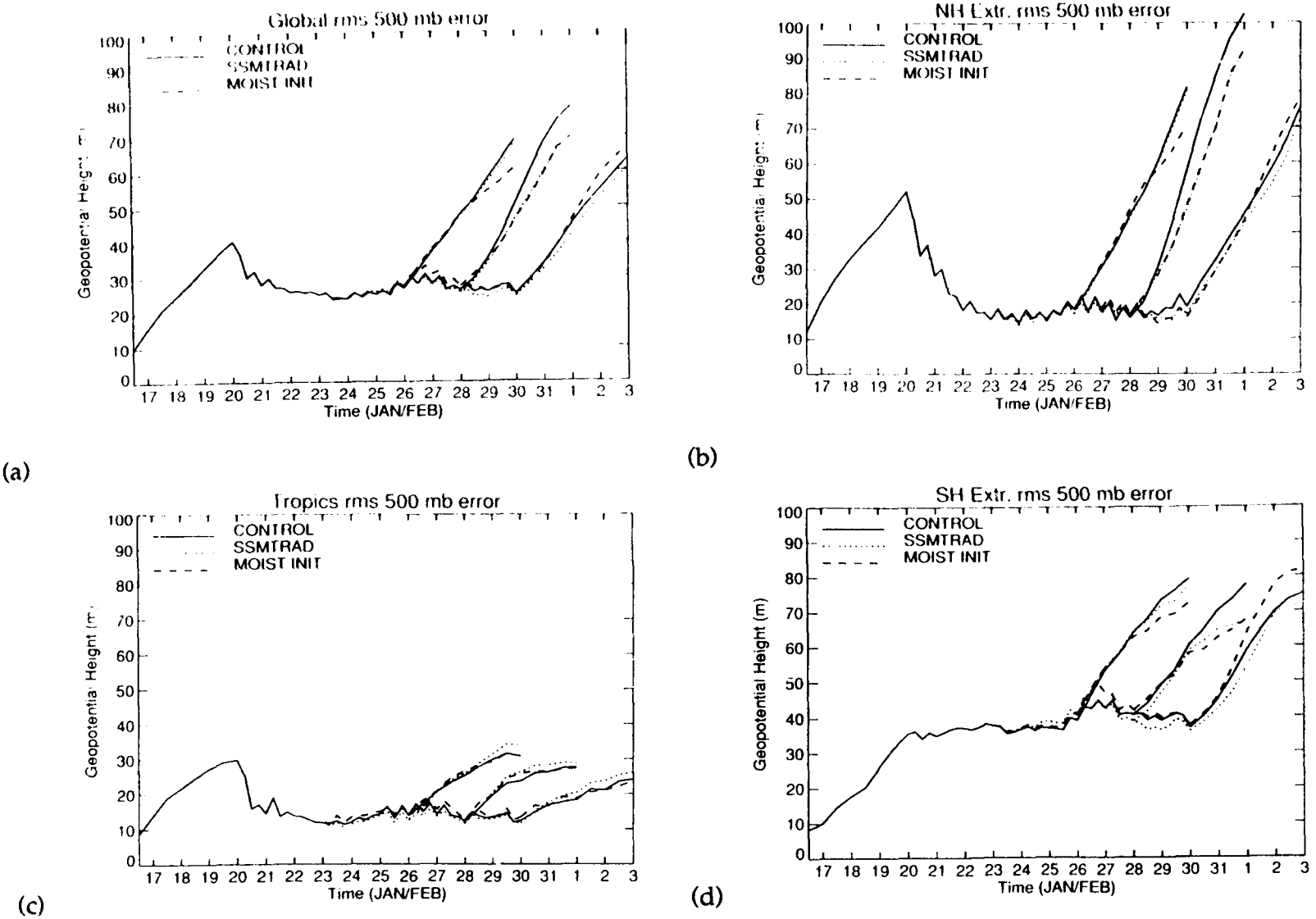

Fig. 6: Root mean square errors of 500 hPa geopotential height computed for the globe (a), Northern Hemisphere extratropics (b), Tropics (c), and Southern Hemisphere extratropics (d). The time period covers the spinup forecast, spinup assimilation, the 7-day assimilation and the 4-day forecasts generated from it.

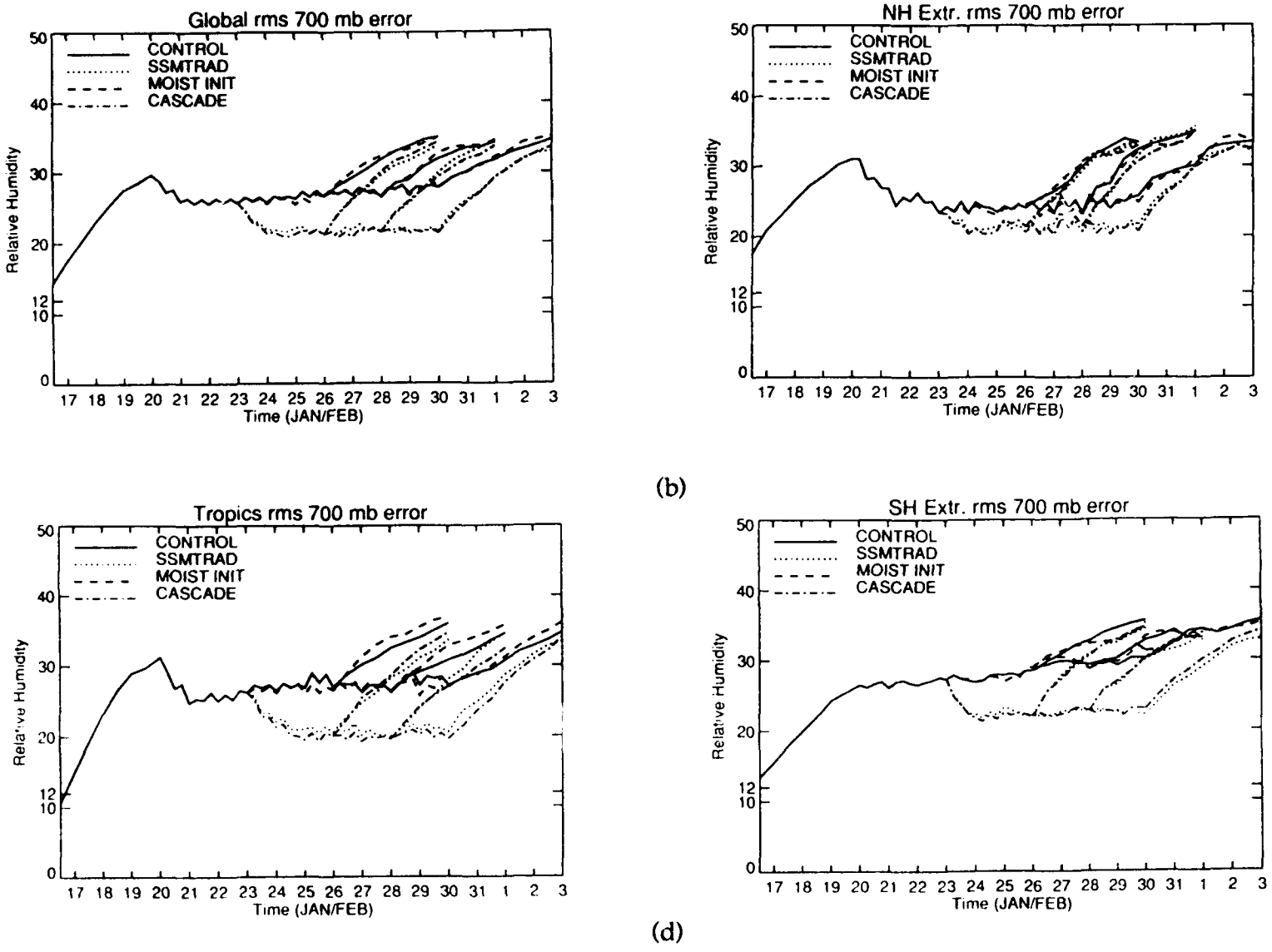

Fig. 7: Root mean square errors of 700 hPa relative humidity computed for the globe (a), Northern Hemisphere extratropics (b), Tropics (c), and Southern Hemisphere extratropics (d). The time period covers the spinup forecast, spinup assimilation, the 7-day assimilation and the 4-day forecasts generated from it.

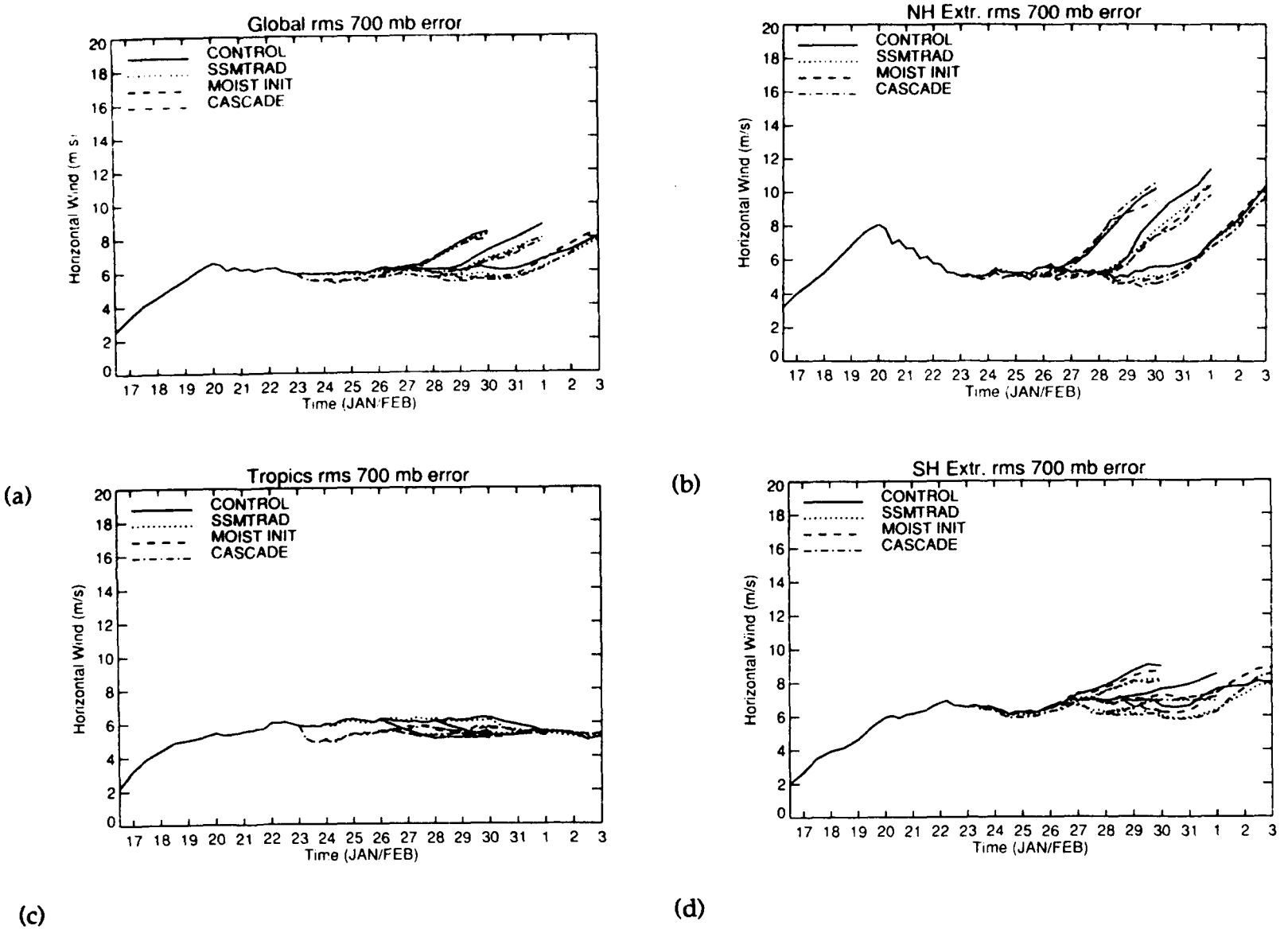

Fig. 8: Root mean square errors of 700 hPa horizontal wind computed for the globe (a), Northern Hemisphere extratropics (b), Tropics (c), and Southern Hemisphere extratropics (d). The time period covers the spinup forecast, spinup assimilation, the 7-day assimilation and the 4-day forecasts generated from it.

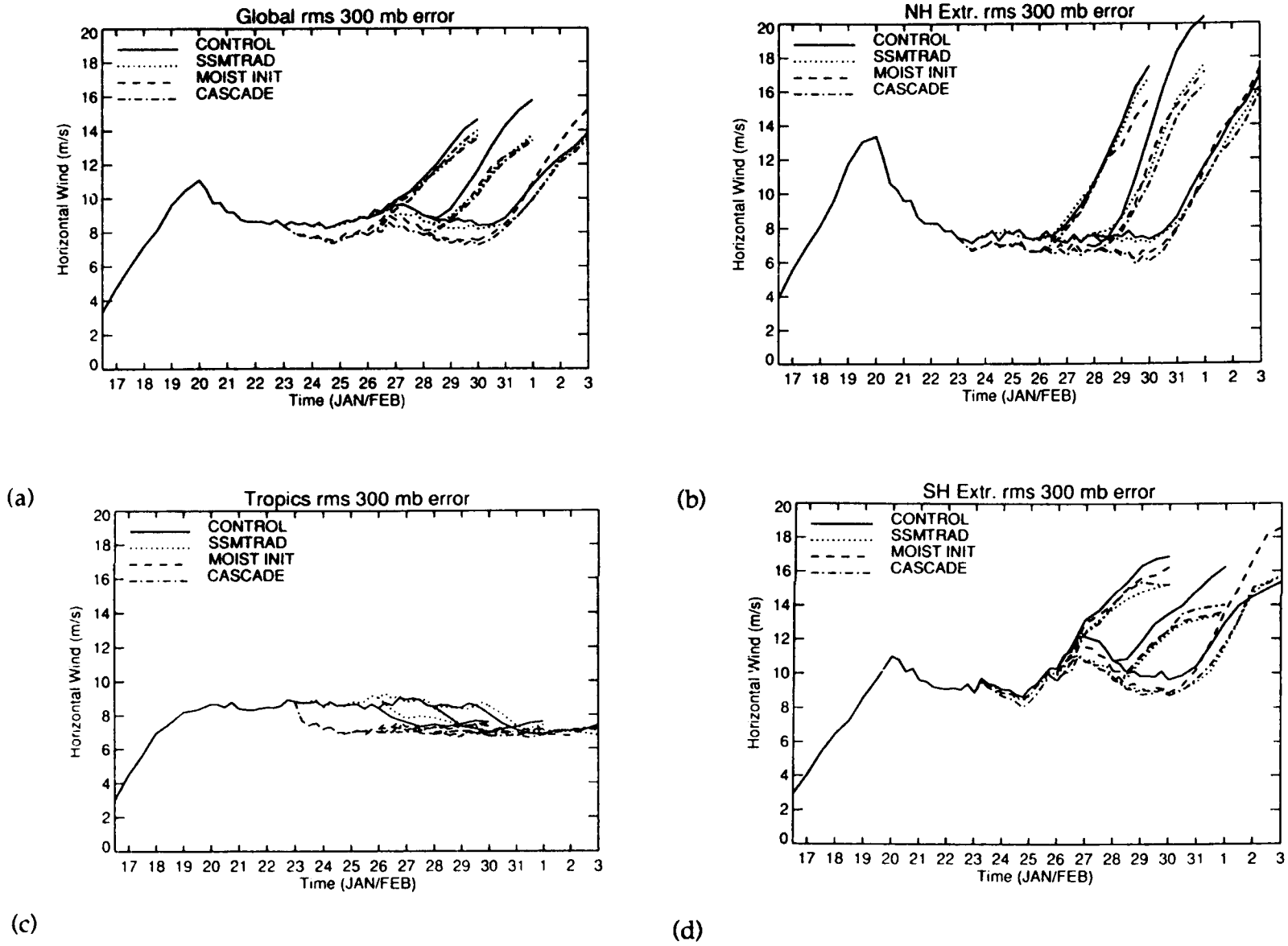

Fig. 9: Root mean square errors of 300 hPa horizontal wind computed for the globe (a), Northern Hemisphere extratropics (b), Tropics (c), and Southern Hemisphere extratropics (d). The time period covers the spinup forecast, spinup assimilation, the 7-day assimilation and the 4-day forecasts generated from it.

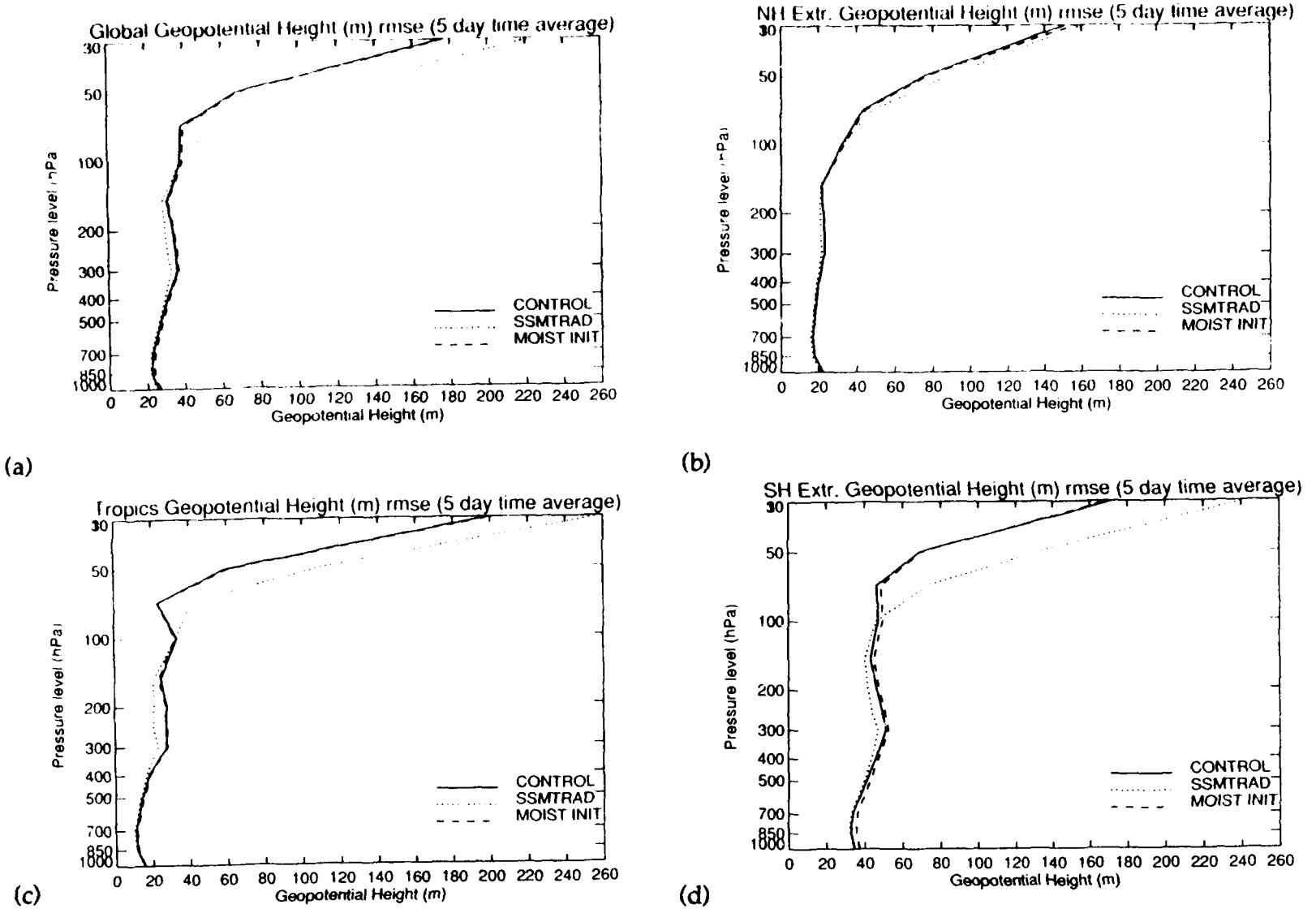

Fig. 10: Vertical profiles of the root mean square errors of geopotential height averaged over the last 5 days of the assimilation, for the globe (a), Northern Hemisphere extratropics (b), Tropics (c), and Southern Hemisphere extratropics (d).

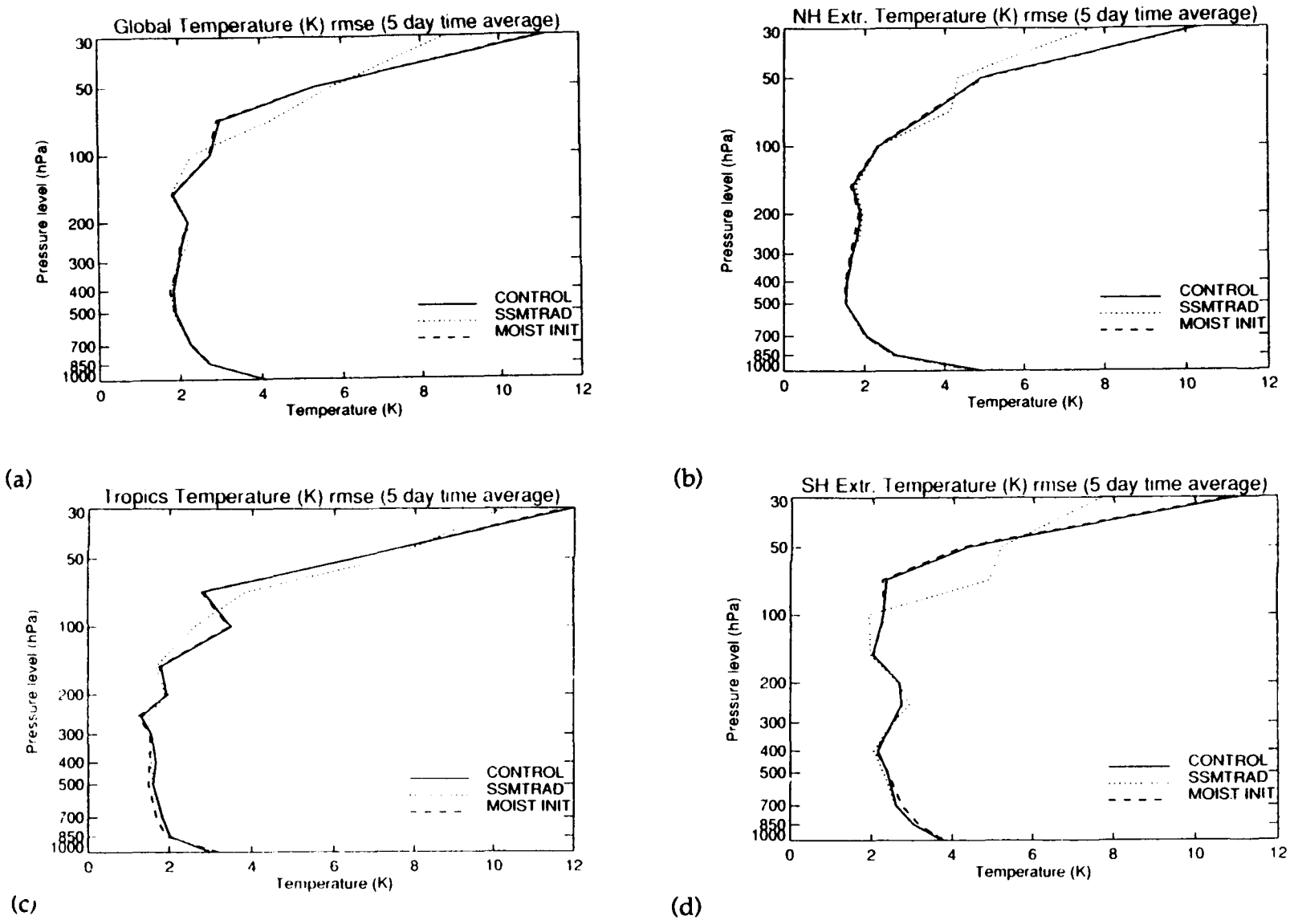

Fig. 11: Vertical profiles of the root mean square errors of temperature averaged over the last 5 days of the assimilation, for the globe (a), Northern Hemisphere extratropics (b), Tropics (c), and Southern Hemisphere extratropics (d).

Relative humidity errors (Fig. 12) are smallest near the surface, and show little variation between 700 hPa and 300 hPa. *Rh* values above 300 hPa were available both from the nature run and our analyses, but since there are virtually no data at those levels those values are not displayed here.

The error profile for the horizontal wind (Fig. 13) has a distinct maximum at the jet level, which is most pronounced in the extratropics. Error magnitudes at that level are approximately 7 m/s in the Northern Hemisphere, and 11 m/s in the Southern Hemisphere.

The performance of the CONTROL data assimilation system can be compared with that of previous OSSEs (Hoffman *et al.*, 1989; Hoffman *et al.*, 1990, Grassotti *et al.*, 1989; and Grassotti *et al.*, 1991, denoted H89, H90, G89, and G91 in the following) using the Phillips Laboratory data assimilation system. The first set of these OSSEs, denoted STATSAT, SSM, SSM+TOVS, WINDSAT in H89, G89, and H90, was designed to assess the impact of statistical retrievals of temperature and moisture from SSM/T measurements, both in combination with and as a replacement for TOVS statistical retrievals, and of an active Doppler Lidar wind sounder. The second set, denoted CONTROL and LIDAR in G91, used the same OI, but with the same improvements in the use of RAOB data and the surface pressure analysis that are being utilized in our present OSSEs (the LIDAR OSSE used simulated data from a scaled down version of the instrument simulated in WINDSAT). Neither of the two previous sets used the new physics packages in the GSM, and they both were run at an R30 and 12-layer resolution.

The present CONTROL OSSE corresponds most closely to the STATSAT experiment of G89 and the CONTROL experiment of G91. The results of the two CONTROL experiments are quite similar: 500 hPa height and 850 hPa and 200 hPa zonal wind analysis errors show identical behavior and have roughly the same magnitudes. Rh analysis errors are slightly smaller in the present CONTROL, particularly in the tropics, because of the improved forecast model (since only RAOB data is used in the moisture analysis, the first guess field has a large effect on the analysis). By contrast, the STATSAT experiment described in H89 suffered from a suboptimal use of RAOB data and a poor surface pressure analysis, resulting in large analysis errors: height errors of 35 m at 500 hPa, compared to 28 m in the present CONTROL; zonal wind errors approximately 1m/s larger than in CONTROL; and *rh* errors approximately 2% larger than in CONTROL.

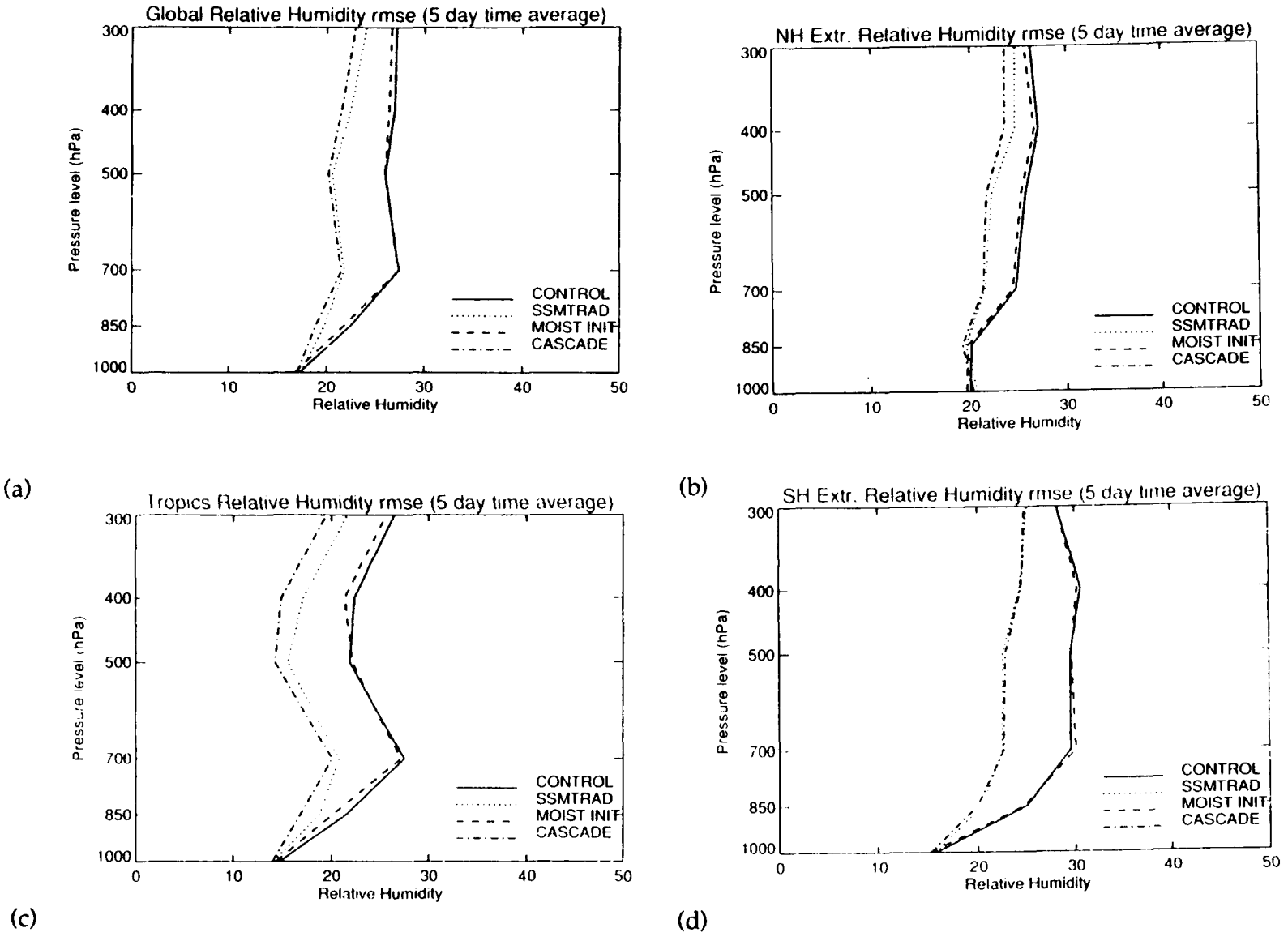

Fig. 12: Vertical profiles of the root mean square errors of relative humidity averaged over the last 5 days of the assimilation, for the globe (a), Northern Hemisphere extratropics (b), Tropics (c), and Southern Hemisphere extratropics (d).

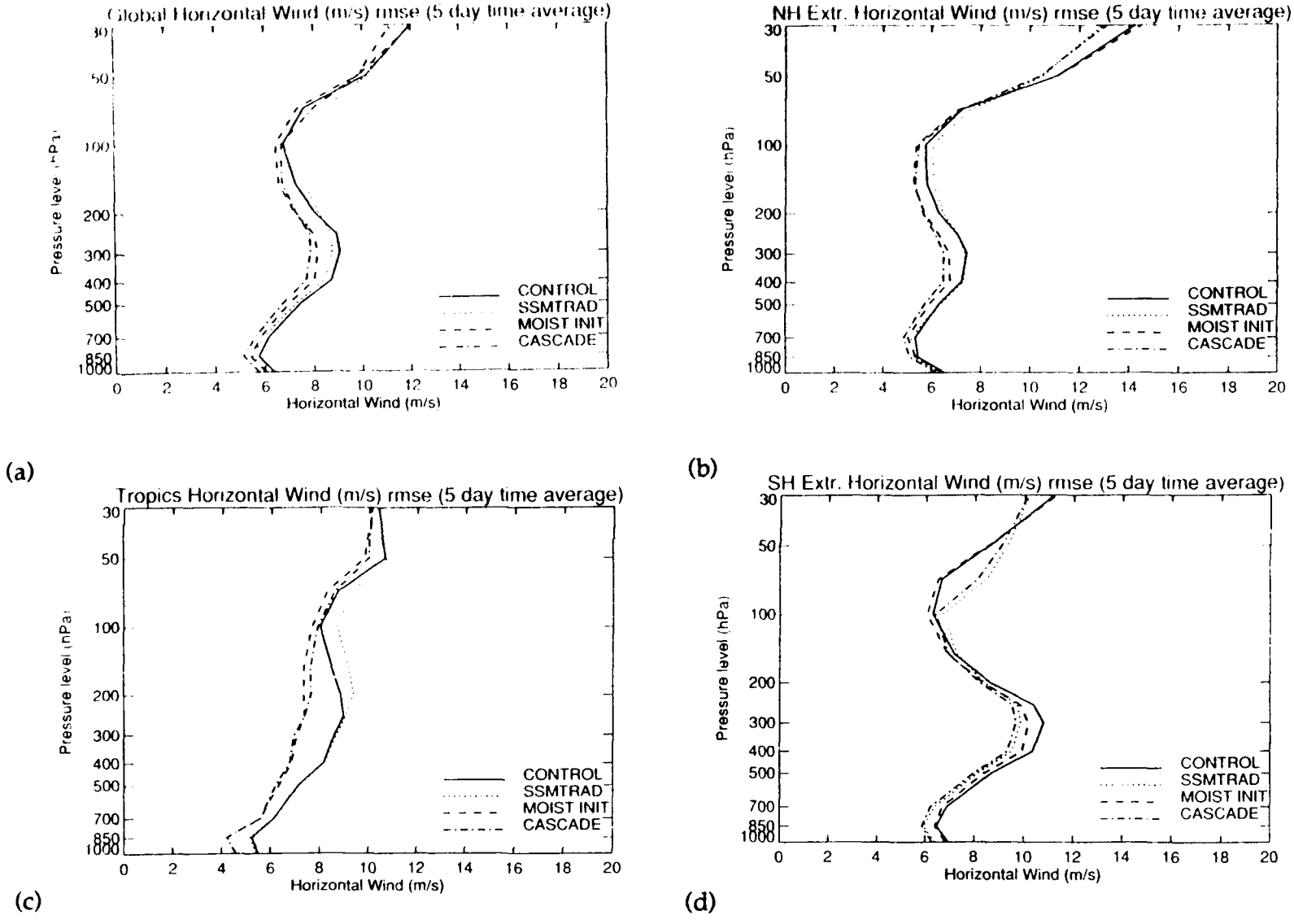

Fig. 13: Vertical profiles of the root mean square errors of the horizontal wind (vector difference) averaged over the last 5 days of the assimilation, for the globe (a), Northern Hemisphere extratropics (b), Tropics (c), and Southern Hemisphere extratropics (d).

4.2 OSSE impacts

In the following discussion of analysis errors, one must bear in mind that these analyses have been initialized, either by the adiabatic NMI (for the CONTROL and SSMTRAD OSSEs), or by the moist initialization procedure (for the MOIST INIT and CASCADE OSSEs). The impacts seen in the analysis errors are thus due to the combined effects of the improved first guess and additional data available to the analysis, and the initialization procedure. The regions for which statistics are presented in the following are defined such that "Tropics" only includes points between 20°S and 20°N; since the moist initialization procedure was applied to points equatorward of 30°, this also affected statistics for the regions denoted "extratropics", which include points between 20° and 80°.

The addition of SSM/T data (in the SSMTRAD OSSE) and/or the moist initialization procedure (in the MOIST INIT and CASCADE OSSEs) have no effect on the 500 hPa height analysis errors (Fig. 6). From Fig. 10 it can be seen that this is true for all levels at and below 500 hPa; outside the Northern Hemisphere, there is a slight positive impact of the SSM/T data below 100 hPa. However, a substantial negative impact is evident above 100 hPa. The corresponding profiles of temperature (Fig. 11) show zero global impact of the moist initialization procedure, with a slight improvement in the tropics below 300 hPa, and a slight degradation in the Southern Hemisphere. The SSM/T data has little or no effect below 300 hPa, a positive impact at 100 and 30 hPa, but a small negative impact at 250 hPa, and a substantial negative impact at 70 and 50 hPa. These SSM/T impacts are consistent with the retrieval error statistics discussed in Appendix B, except that the degradation in the stratosphere introduced at each retrieval time period is smaller than the accumulated effect evident in the SSMTRAD analysis errors.

The relative humidity errors show a clear and positive effect of the additional SSM/T data, both in the 700 hPa time series (Fig. 7) and in the vertical profiles of *rh* error (Fig. 12). *Rh* errors are reduced by up to 10% (from 30% to 20%) in the Southern Hemisphere, whereas impacts are smaller (around 5%) in the Northern Hemisphere. Interestingly, the *rh* error reduction computed from the retrieval statistics (see Appendix B) shows reductions that increase with height, whereas the cumulative effects shown in Fig. 12 are largest at 700 and 500 hPa.[4]

---

[4]The rh analyses in the stratosphere (not shown here) are generally poorer in the SSMTRAD OSSE. Since the SSM/T retrievals of moisture are only available at and below 300 hPa, this degradation is caused by changes to the temperature and, indirectly, the wind fields.

The moist initialization has a very small impact on *rh* errors in the tropics in the MOIST INIT OSSE (less than a 1% error reduction). From Fig. 7 it can be seen that a larger impact exists during the first 3 days of MOIST INIT. In the CASCADE OSSE, the positive impact persists throughout the seven day period, and the CASCADE OSSE consequently has the lowest *rh* errors in the tropics. Outside the tropics, there is little difference between the SSMTRAD and CASCADE *rh* errors.

The largest effect of the moist initialization is evident in the tropical wind fields (Fig. 13), where errors are reduced by as much as 2 m/s (MOIST INIT, CASCADE vs. CONTROL, SSMTRAD). Improvements are smaller, but still noticeable, in the extratropics. This is consistent with the off-line tests of the moist initialization procedure discussed in Appendix C. In the Southern Hemisphere, the SSM/T data also improves the wind field below 150 hPa (SSMTRAD vs. CONTROL). A degradation of the horizontal winds is evident in SSMTRAD at and above the tropopause in all regions; this is related to the degradation of the temperature and height fields at those levels discussed above. The wind errors of the CASCADE OSSE are in general equal to the smaller of SSMTRAD or MOIST INIT, except in the Northern Hemisphere where CASCADE errors are slightly smaller than any of the other OSSEs. Time series of the 700 hPa and 300 hPa horizontal wind errors (Fig. 8 and 9) show that effects evident in the 5-day averages are typical of the impacts throughout the 7-day assimilation.

In summary, the analysis errors indicate a small positive impact of SSM/T data on tropospheric temperatures in the tropics and Southern Hemisphere, a positive impact on tropospheric winds in the Southern Hemisphere, and a large positive impact on *rh* in the tropics and the Southern Hemisphere. A negative impact of the SSM/T data is evident in the temperature, height, and wind fields in the lower stratosphere. The moist initialization lowered errors in the wind fields, particularly in the tropics, and *rh* errors in the tropics. With the exception of the lower stratosphere, the CASCADE OSSE resulted in the lowest analysis errors overall, both because positive impacts from the MOIST INIT and SSMTRAD complement each other, and because in some cases (e.g., tropical *rh*) positive impacts are partially additive.

The analysis errors discussed up to now, while of interest by themselves, also affect the quality of the ensuing forecasts. The forecast errors for the individual forecasts are shown in Fig. 6 - 9, and average errors from the day 3, 5, and 7 forecasts are shown in Fig. 14- 17. As might be expected from the analysis error impacts, there is no consistent impact on the 500 hPa height errors: while the averaged forecast errors show a positive impact for SSMTRAD and MOIST INIT, examination of the individual forecasts indicates near zero or negative impacts for one or two of the three forecasts. *Rh* errors at 850 hPa show positive impacts of SSM/T data in the Southern Hemisphere, where SSMTRAD and CASCADE are smaller by 5% (at the

initial time) to 1% (at 3 days). By the fourth day of the forecast there is no impact. In the tropics, CASCADE forecast errors are smaller than either SSMTRAD or MOIST INIT during the first 1 to 2 days of the forecast. The *rh* forecast improvements are evident in all three forecasts.

Finally, forecast errors of zonal wind at 850 hPa and 200 hPa reflect the improvements to the Southern Hemisphere wind analyses in SSMTRAD, and the tropical wind analyses in MOIST INIT. The latter does not persist past the first day of the forecast, whereas the Southern Hemisphere 850 hPa wind field errors are smaller throughout the forecast period in SSMTRAD. In the Northern Hemisphere the averaged forecast errors seem to indicate a positive impact beyond 2 days, but, as in the case of the 500 hPa heights, this impact is not evident in all 3 forecasts and is most likely due to sampling limitations.

Compared to our previous OSSEs using SSM/T data, impacts seen here are generally smaller due to the smaller errors of the CONTROL experiment. In particular, the small positive impact on Northern Hemisphere heights (2-3 m) seen in G89 is absent here, and *rh* analysis error improvements of 5% are only 3-4% here; forecast *rh* error improvements in G89 decreased to 2% at day 4, compared to 0% at day 2 here; however, the absolute error magnitudes are smaller because of the improved analysis and forecast model. Rh forecast errors in particular were saturating near 30% in G89, whereas the present error curves have not flattened out by day 4, when they reach 28%.

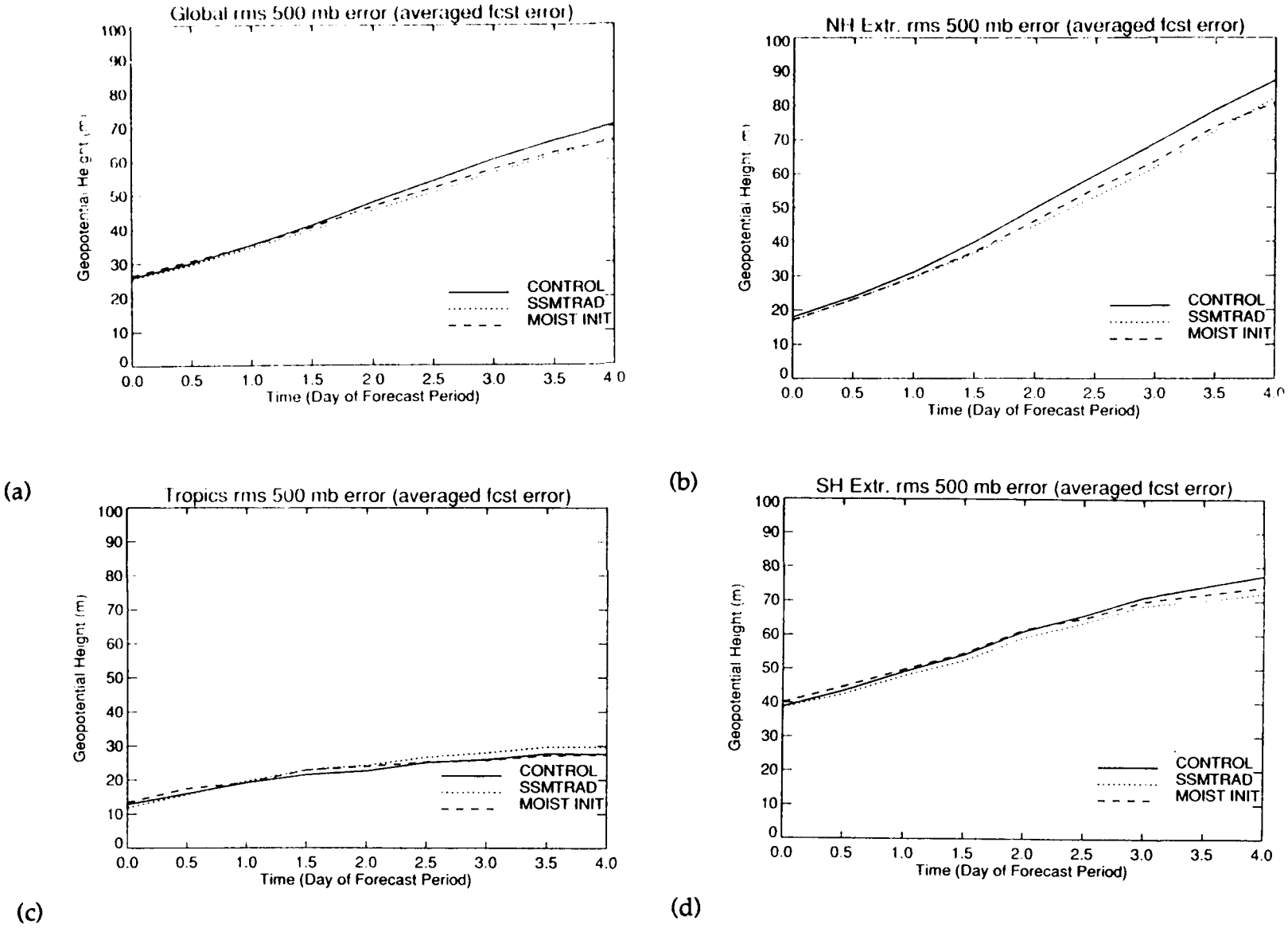

Fig. 14: Root mean square errors of 500 hPa geopotential height as a function of forecast lead time, averaged over the day 3, 5, and 7 forecasts, for the globe (a), Northern Hemisphere extratropics (b), Tropics (c), and Southern Hemisphere extratropics (d).

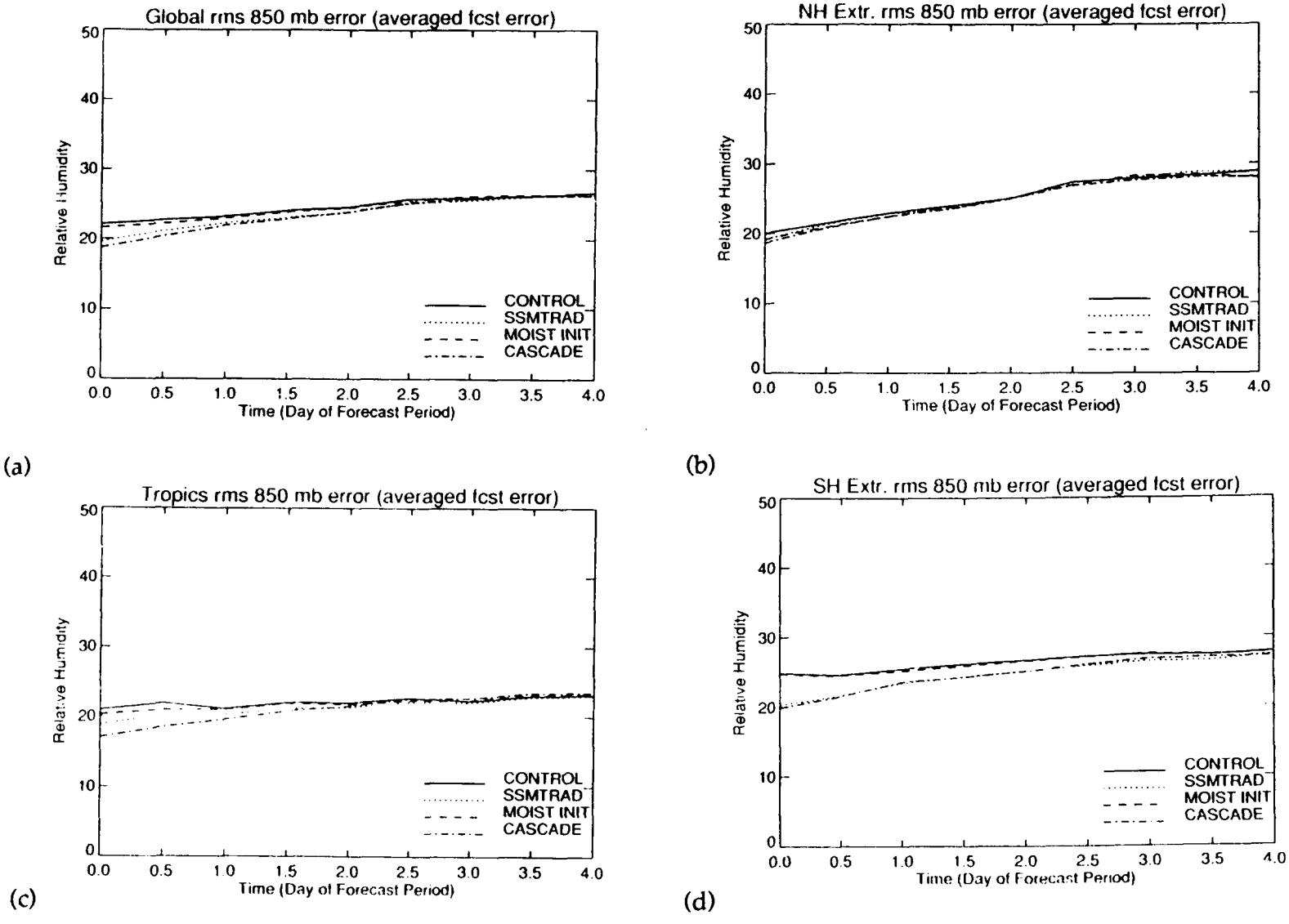

Fig. 15: Root mean square errors of 850 hPa relative humidity as a function of forecast lead time, averaged over the day 3, 5, and 7 forecasts, for the globe (a), Northern Hemisphere extratropics (b), Tropics (c), and Southern Hemisphere extratropics (d).

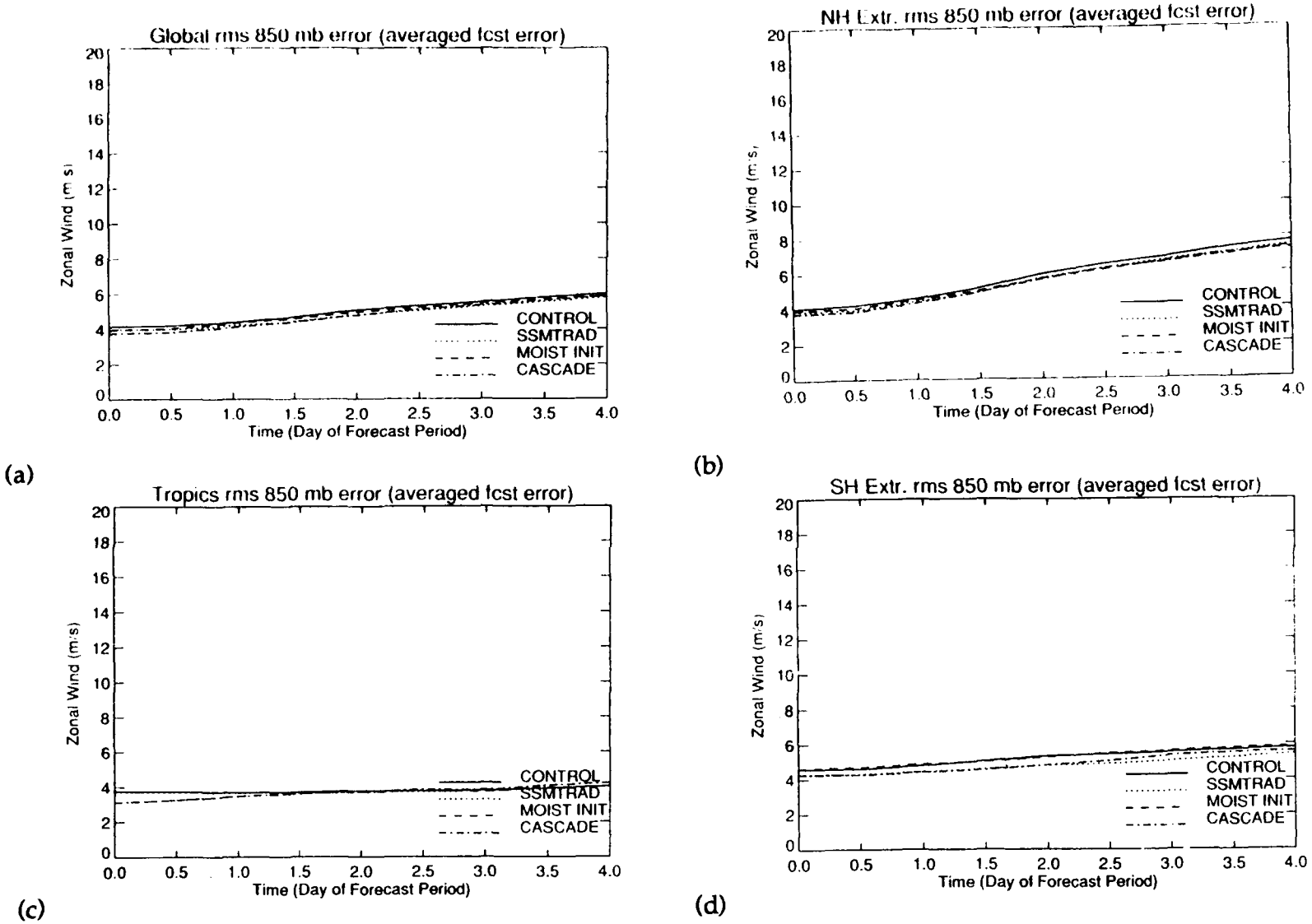

Fig. 16: Root mean square errors of 850 hPa zonal wind as a function of forecast lead time, averaged over the day 3, 5, and 7 forecasts, for the globe (a), Northern Hemisphere extratropics (b), Tropics (c), and Southern Hemisphere extratropics (d).

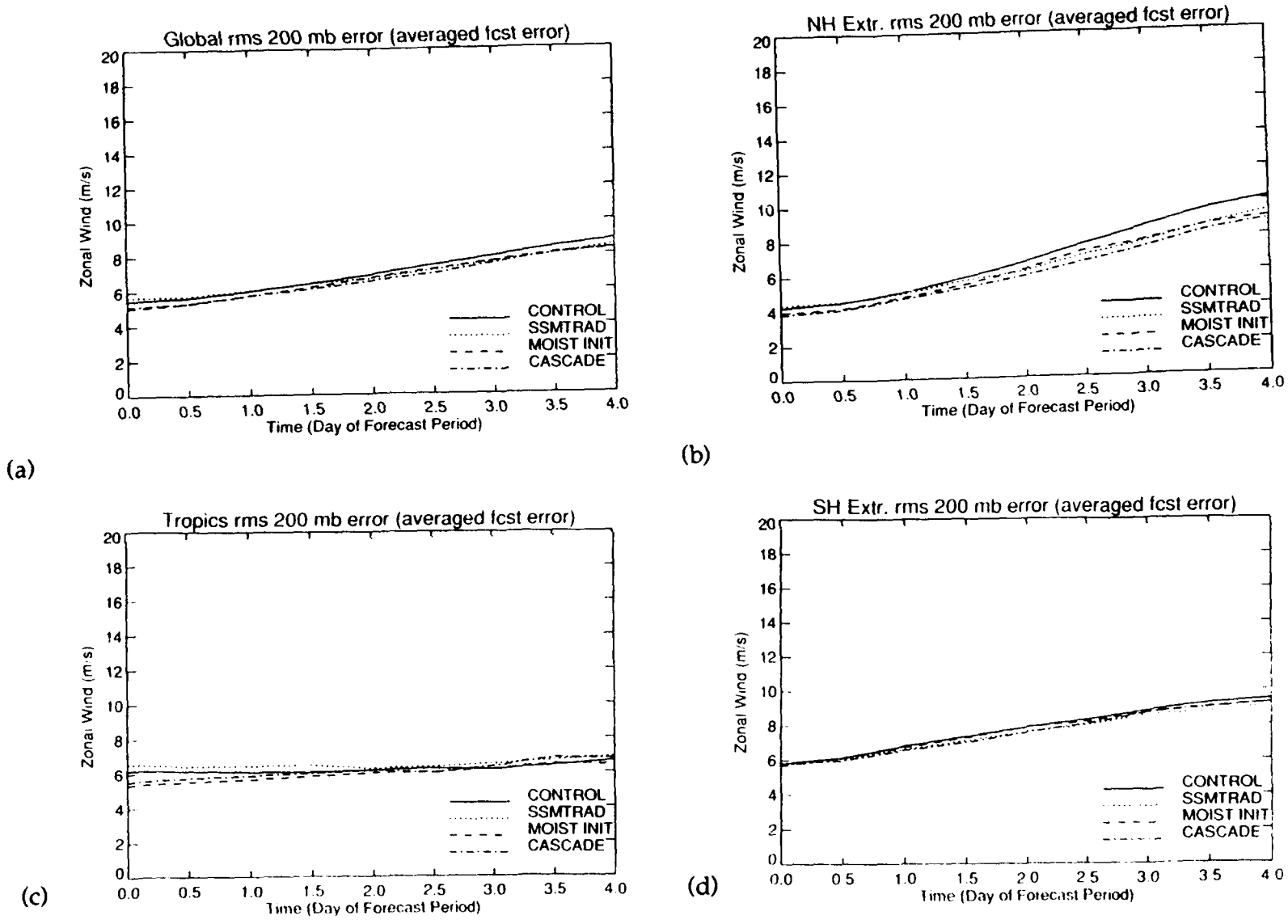

Fig. 17: Root mean square errors of 200 hPa zonal wind as a function of forecast lead time, averaged over the day 3, 5, and 7 forecasts, for the globe (a), Northern Hemisphere extratropics (b), Tropics (c), and Southern Hemisphere extratropics (d).

5 Summary and Conclusions

A set of OSSEs was performed to assess the impact of SSM/T temperature and moisture data, and of a moist initialization procedure making use of observed precipitation rates. The SSM/T data, as well as all the conventional data, were simulated with as realistic errors as possible. The observed precipitation rates, on the other hand, did not include any observational errors, and the results thus represent an upper limit of the positive impact of our particular initialization procedure.

The analysis system used in the CONTROL experiment, which used the full complement of conventional data in an OI assimilation scheme, performed satisfactorily. Comparisons with similar assimilation experiments using earlier versions of the data assimilation system showed the beneficial effects of improvements to the OI (better use of RAOB data and improved surface analysis) and the GSM (higher resolution and more sophisticated physics).

The analysis errors indicate a small positive impact of SSM/T data on tropospheric temperatures in the tropics and Southern Hemisphere, a positive impact on tropospheric winds in the Southern Hemisphere, and a large positive impact on *rh* in the tropics and the Southern Hemisphere. A negative impact of the SSM/T data is evident in the temperature, height, and wind fields in the lower stratosphere.

The moist initialization lowered analysis errors in the wind fields, particularly in the tropics, and *rh* errors in the tropics. With the exception of the lower stratosphere, the CASCADE OSSE, which combined the SSM/T data and the moist initialization, resulted in the lowest analysis errors overall, both because positive impacts from the MOIST INIT and SSMTRAD complement each other, and because in some cases (e.g., tropical *rh*) positive impacts are partially additive.

Forecast errors showed positive impacts in only selected variables and geographical regions. *Rh* errors at 850 hPa show positive impacts of SSM/T data in the Southern Hemisphere, where SSMTRAD and CASCADE are smaller by 5% (at the initial time) to 1% (at 3 days). By the 4th day of the forecast there is no impact. In the tropics, CASCADE forecast errors are smaller than either SSMTRAD or MOIST INIT during the first 1 to 2 days of the forecast. Finally, forecast errors of zonal wind at 850 hPa and 200 hPa reflect the improvements to the Southern Hemisphere wind analyses in SSMTRAD, and the tropical wind analyses in MOIST INIT. The latter does not persist past the first day of the forecast, whereas the Southern Hemisphere 850 hPa wind field errors are smaller throughout the forecast period in SSMTRAD.

Compared to our previous OSSEs using SSM/T data, impacts seen here are generally smaller due to the smaller errors of the CONTROL experiment. In particular, the small positive impact on Northern Hemisphere heights (2-3 m) seen in G89 is absent here, and *rh* analysis and forecast error improvements are smaller here; however, the absolute error magnitudes are smaller because of the improved analysis and forecast model. The negative impact of SSM/T data in the stratosphere was absent in our previous OSSE.

It is remarkable that even the relatively crude moist initialization procedure implemented in the data assimilation scheme in MOIST INIT and CASCADE results in the analysis and initial forecast error improvements seen here, particularly since the spinup behavior of precipitation shown in Appendix C is far from perfect. This suggests that additional improvements might be possible if more sophisticated procedures are employed, and similar approaches applied to large-scale precipitation outside the tropics. It remains to be determined, however, how much the impacts will be modified by the inclusion of realistic measurement errors.

6 References

Atlas, D. and O. W. Thiele, 1981: Precipitation measurements from space. Workshop Report, NASA Goddard Space Flight Center, Greenbelt, MD, 437 pp.

Ballish, B., 1980: Initialization, theory and application to the NMC spectral model. Ph.D. Thesis, Department of Meteorology, University of Maryland

Bergman, K. H., 1979: Multivariate analysis of temperature and winds using optimum interpolation. *Mon. Wea. Rev.*, **107**, 1423-1444.

Dey, C., C. P. Arnold and W. Bostelman, 1985: Design of a WINDSAT observing system simulation experiment. Global Wind Measurements, Deepak, W. E. Baker and R. J. Curran, Eds. pp. 73-79.

Elliott, W. P. and D. J. Gaffen, 1991: On the utility of radiosonde humidity archives for climate studies. *Bull. Amer. Meteor. Soc.*, **72**, 1507-1520.

Eyre, J. R. and H. M. Woolf, 1988: Transmittance of atmospheric gases in the microwave region: A fast model. *Appl. Opt.*, **27**, 3244-3249.

Eyre, J. R., 1989: Inversion of cloudy satellite sounding radiances by non-linear optimal estimation: Theory and simulation for TOVS. *Quart. J. Roy. Meteor. Soc.*, **115**, 1001-1026.

Falcone, V. J. and R. G. Isaacs, 1987: The DMSP microwave suite (1987). Proceedings, NOAA Conference on Passive Microwave Observing from Environmental Satellites, pp. 174-185.

Grassotti, C., R. Isaacs, R. N. Hoffman, J.-F. Louis, T. Nehrkorn and M. Mickelson, 1989: A study of the impact of simulated 183 GHz water vapor retrievals on numerical weather prediction. AFGL-TR-89-0093. AFGL, Hanscom AFB, MA. 173 pp. [NTIS ADA210431]

Grassotti, C., R. G. Isaacs, R. N. Hoffman, M. Mickelson, T. Nehrkorn and J.-F. Louis, 1991: A simple Doppler wind LIDAR sensor: Simulated measurements and impacts in a global assimilation and forecast system. Scientific Report No. 1, PL-TR-91-2253. Phillips Laboratory, AF System Command, Hanscom AFB, MA 01731. 87 pp.

Halberstam, I. and S.-L. Tung, 1984: Objective analysis using Hough vectors evaluated at irregularly spaced locations. *Mon. Wea. Rev.*, **112**, 1804-1817.

Hayden, C. M. and R. J. Purser, 1988: Three-dimensional recursive filter objective analysis of meteorological fields. *CIMSS View.*, **4**, 1-5.

Hoffman, R. N., C. Grassotti, R. G. Isaacs, J.-F. Louis and T. Nehrkorn, 1990: Assessment of the Impact of Simulated Satellite Lidar Wind and Retrieved 183 GHz Water Vapor Observations on a Global Data Asssimilation System. *Mon. Wea. Rev.*, **118**, 2513-2542.

Hoffman, R. N., R. G. Isaacs, J.-F. Louis, T. Nehrkorn and M. Mickelson, 1989: Satellite enhanced numerical weather prediction. AFGL-TR-89-0099. AFGL, Hanscom AFB. MA. 116 pp. [NTIS ADA210108]

Hoffman, R. N., M. Mickelson and T. Nehrkorn, 1988: Enhancements to the AFGL Statistical Analysis Program (ASAP) for the global multivariate analysis of heights and winds. AFGL-TR-87-0279. AFGL, Hanscom AFB. MA. 110 pp. [NTIS ADA202912]

Isaacs, R. G., 1987: A unified retrieval methodology for the Defense Meteorological Satellite Program meteorological sensors. Int'l Workshop on Remote Sensing Retrieval Methods, Williamsburg, VA, December 1987, pp. 15-18.

Julian, P. R., 1984: Objective analysis in the tropics: A proposed scheme. *Mon. Wea. Rev.*, **112**, 1752-1767.

Kasahara, A., R. C. Balgovind and B. B. Katz, 1988: Use of Satellite Radiometric Imagery Data for Improvement in the Analysis of Divergent Wind in the Tropics. *Mon. Wea. Rev.*, **116**, 866-883.

Koch, S. E., M. DesJardins and P. J. Kocin, 1983: An Interactive Barnes Objective Map Analysis Scheme for Use with Satellite and Conventional Data. *J. Climate Appl. Meteor.*, **22**, 1487-1503.

Liou, K.-N., S.-C. Ou, S. Kinne and G. Koenig, 1984: Radiation parameterization program for use in general circulation models. AFGL-TR-84-0217. AFGL, Hanscom AFB, MA. [NTIS ADA148015]

Louis, J.-F., R. N. Hoffman, T. Nehrkorn and D. Norquist, 1989: Observing systems experiments using the AFGL four-dimensional data assimilation system. *Mon. Wea. Rev.*, **117**, 2186-2203.

Mahrt, L., H.-L. Pan, P. Ruscher and C.-T. Chu, 1987: Boundary layer parameterization for a global spectral model. AFGL-TR-87-0246. AFGL, Hanscom AFB, MA. 188 pp. [NTIS ADA199440]

Martin, D. W. and W. D. Scherer, 1973: Review of satellite rainfall estimation methods. *Bull. Amer. Meteor. Soc.*, **54**, 661-674.

McPherson, R. D., 1984: Cloud drift wind estimates during FGGE. Report No. 288. NMC, Washington, DC. 13 pp.

McPherson, R. D., K. H. Bergman, R. E. Kistler, G. E. Rasch and D. S. Gordon, 1979: The NMC operational global data assimilation system. *Mon. Wea. Rev.*, **107**, 1445-1461.

Mohanty, U. C., A. Kasahara and R. Errico, 1986: The Impact of Diabatic Heating on the Initialization of Divergent Circulations in a Global Forecast Model. *J. Meteor. Soc. Japan.* **64**, 805-817.

Nastrom, G. D. and K. S. Gage, 1985: A climatology of atmospheric wavenumber spectra of wind and temperature observed by commercial aircraft. *J. Atmos. Sci.*, **42**, 950-960.

Nastrom, G. D., K. S. Gage and W. H. Jasperson, 1984: Kinetic energy spectrum of large- and mesoscale atmospheric processes. *Nature.* **310**, 36-38.

Nehrkorn, T., R. Hoffman, J.-F. Louis and M. Zivkovic, 1992: An enhanced global spectral model. PL-TR-92-2011. Geophysics Directorate, Phillips Lab., Hanscom AFB, MA 01731. 52 pp. [NTIS ADA251242]

Norquist, D. C. (1982). Development of objective analysis scheme using the method of optimum interpolation. In *Objective Analysis and Prediction Techniques.* AFGL-TR-82-0394. AFGL, Hanscom AFB, MA. A. M. Gerlach, Ed. 51-55. [NTIS ADA131465]

Norquist, D. C. (1983). Development and testing of a multivariate global statistical analysis system. In *Objective Analysis and Prediction Techniques.* AFGL-TR-83-0333. AFGL, Hanscom AFB, MA. A. M. Gerlach, Ed. 10-48. [NTIS ADA142441]

Norquist, D. C., 1984: Users guide for optimum interpolation method of global data assimilation. AFGL-TR-84-0290. AFGL, Hanscom AFB, MA. 67 pp. [NTIS ADA155929]

Norquist, D. C., 1986: Alternative forms of moisture information in 4-D data assimilation. AFGL-TR-86-0194. AFGL, Hanscom AFB, MA. 144 pp. ADA129792

Norquist, D. C., 1988: Alternate forms of humidity information in global data assimilation. *Mon. Wea. Rev.*, **116**, 452-471.

Puri, K., 1983: The relationship between convective adjustment, Hadley circulation and normal modes of the ANMRC spectral model. *Mon. Wea. Rev.*, **111**, 23-33.

Puri, K., 1985: Sensitivity of low-latitude velocity potential field in a numerical weather prediction model to initial conditions, initialization and physical processes. *Mon. Wea. Rev.*, **113**, 449-466.

Puri, K., W. Bourke and R. Seaman, 1982: Incremental linear normal mode initialization in four-dimensional dat assimilation. *Mon. Wea. Rev.*, **110**, 1773-1785.

Rasch, P. J., 1985a: Developments in normal mode initialization. Part I: a simple interpretation for normal mode initialization. *Mon. Wea. Rev.*, **113**, 1746-1752.

Rasch, P. J., 1985b: Developments in normal mode initialization. Part II: a new method and its comparison with currently used schemes. *Mon. Wea. Rev.*, **113**, 1753-1770.

Rodgers, C. D., 1990: Characterization and error analysis of profiles retrieved from remote sounding measurements. *J. Geophys. Res.*, **95**(D5), 5587-5595.

Seaman, R. S., 1989: Tuning the Barnes Objective Analysis Parameters by Statistical Interpolation Theory. *J. Atmos. Ocean. Tehnol.*, **6**, 993-1000.

Slingo, J. M., 1987: The development and verification of a cloud prediction scheme for the ECMWF model. *Quart. J. R. Meteor. Soc.*, **113**, 899-928.

Soong, S.-T., Y. Ogura and W.-S. Kau, 1985: A study of cumulus parameterization in a global circulation model. AFGL-TR-85-0160. AFGL, Hanscom AFB, MA. 113 pp. [NTIS ADA170137]

Appendix A: Data Simulation Methodology for the Standard Observations

A.1 Representativeness of the nature data.

Scales on the order of 15 minutes to an hour or two are not in the nature data because of model resolution; similarly for scales from 25 km to 100 km. These scales do affect the observing systems (RAOBs and SATEMs for example). These scales should be "added" to the nature data before sampling it or otherwise simulated. Simulating this effect essentially adds errors to the observations. We have added a random component of the proper size to each perfect observation. These need not be correlated horizontally since the correlation length scale is so small for these scales. It is also unclear whether these errors should have any vertical correlations, so we have not introduced any vertical correlations. The proper size of these errors was determined using an energy spectrum of $E=de/dk=c\ k^{\gamma}$, with $\gamma=-5/3$, deduced from observed atmospheric spectra (Nastrom and Gage, 1985; Nastrom *et al.*, 1984). Since different instruments average over different space-time volumes, differently sized errors were used for each data type.

The proportionality constant c was obtained by fitting this equation to values in Nastrom's table, using entries for all flights. The variance under this curve was then determined between the wavenumbers $2\pi/L_1$ and $2\pi/L_2$, where L_1 is the resolution of the nature run (T106 = 310 km), and L_2 the averaging length scale of the instrument. There is less than a 10% change in the standard deviation for L_2 going from 20 km to 0 km. Resulting values are:

winds = 1.9 m/s for troposphere (below 100 hPa), 2.0 m/s (100 hPa and above)

temperature = .8 K for troposphere , 1.8 K for stratosphere (this value was not used, because it might have been caused by aircraft bobbing)

No attempt was made to compensate for the smoothing of the highest resolved wavenumbers in the ECMWF nature run. It was decided that the uncertainty in the observed spectra did not warrant this. The temperature values are not used explicitly in the simulation of the RAOBs, although the temperature errors resulting from the specified height errors seem to be of the right magnitude.

A.2 Time interpolation.

The perfect data that are being sampled are at the synoptic times (0, 6, 12 and 18 GMT) for the data within plus or minus 3 hours of these times. To interpolate properly in time one would need to do twice as much work as without time interpolation. For example for AIREPs at 4 GMT one would need to create perfect data at 0 GMT for the 6 GMT data locations. Similarly

for reports at 8 GMT we would also need to process the 6 GMT data against the 12 GMT nature file. It might be sufficient to interpolate the 12 - 00 GMT nature run difference to the 6 GMT observations.

It might be best to perform such a time interpolation. It would also be better to improve ASAP to calculate observation increments which interpolate the first guess to each observing time. This is the nominal but unaffordable case, and there are several alternative approaches. The first alternative is to do just the time interpolation and not modify ASAP. A second alternative is to simulate the effect of the time interpolation by adding errors to the observations of the same size as those introduced by ASAP in not performing its own time interpolation. ASAP would also be left unchanged in this scenario. The third alternative is to simulate improving ASAP by not adding any time interpolation errors.

If we followed the second alternative, we could, as an approximation, increase the magnitude of the errors associated with for the off-time observations. Of course the errors due to timeliness are correlated. The size of these errors could be estimated by processing one time period including time interpolation. Alternatively, we could examine the size of persistence forecast errors for 1, 2 and 3 hours. This would be simpler and give us stable statistics at all latitudes and over the ocean. The original simulated errors could then be amplified by different factors for different time lags and latitude (differently for ocean and land perhaps) so that the standard deviations are correct.

After discussion with the contract monitor, we decided to adopt the third alternative, which is by far the simplest to implement.

A.3 Measurement error

The measurement error varies with data type, and they are simulated as follows:

A.3.1 Type 1: Raobs, Pibal, etc.

Errors are expected to be uncorrelated horizontally between pairs but correlations in the vertical are expected. We obtained the correlations from the statistics used in the ECMWF OI scheme. We performed an eigenvector (or EOF) analysis of the covariance matrix to simulate the height errors. From those, layer temperature errors were derived hydrostatically, and mandatory and significant level temperature error were derived that were consistent with the layer temperature errors. Wind errors were specified using the EOFs of its vertical covariance matrix, and interpolated to significant levels as needed. *Rh* errors were specified as uncorrelated random numbers, using instrument errors from Elliott and Gaffen (1991) plus an assumed 10% error of representativity. Note that these instruments do not sample nature instantaneously. A radiosonde ascent to 100 hPa takes on the order of one

hour or more. However, as discussed above, we did not explicitly treat the time interpolation errors of any of the observations.

A.3.2 Type 2: Aireps.

Potential height assignment errors and instrument biases can introduce horizontally correlated errors for individual aircraft. However, aircraft ID is not saved in our data sets so it would be difficult to simulate this. Since the numbers of observations is so small, and there is also little guidance in the choice of proper correlation lengths, we just used random Gaussian errors for u and v and T. Instrument errors were taken from Hoffman et al. (1990)

A.3.3 Type 4: Satems.

Statistical satellite retrievals for TOVS were calculated in simulation by performing a forward problem computation and a statistical retrieval. Retrievals were only computed over water, and equatorward of 65 degrees (to avoid complications of surface emissivity over land and ice).

The forward model code was obtained from Jon Eyre. The input profile to the forward problem consists of nature run temperature and rh profiles (at the 14 mandatory levels), bilinearly interpolated to the sounding location from a 1 by 1 degree nature run data set and surface values of pressure, temperature, rh, and u and v (the latter obtained using routine GETSFC from the GSM preprocessor), along with an effective cloud cover. The cloud cover is taken as the maximum of the parameters PCC1 and PCC2 from the original (real) retrievals. Errors of representativity appropriate for the 125 km averaging length scale of the retrievals are added to the nature run data before input to the forward problem. The mandatory level data is then interpolated and extrapolated to the 40 (15 for moisture) forward problem levels. The interpolation matrices have been derived from a data base of retrieval profiles provided by McMillan (NESDIS). Instrument errors are added to the computed radiances.

The statistical retrieval used a D-matrix that has been computed from an independent sample of nature run data (the 4 days from Jan. 16 to Jan. 20, 1979). Separate D-matrices were derived for "clear" and "cloudy" retrievals, but no further stratification was done. The geometry is not explicitly simulated: the forward problem was done for the HIRS and MSU channels, using the exact same profile, and nadir conditions were assumed for all retrievals. Separation between clear and cloudy retrievals were based on a single cutoff value for cloud cover, and not the more complicated criterion used in the actual retrievals (based on the number of cloud-free HIRS IFOVs); similarly, the "mixed" retrieval were not simulated. The threshold was selected based on the reported distribution of cloudy and clear retrievals, and the distribution of max(PCC1, PCC2).

The retrieved profiles of temperature were then converted to layer mean temperatures and/or layer thicknesses, depending on the format of the perfect observation, and layer precipitable water. Note that the moisture retrievals are not used by our OI.

A.3.4 Type 6: CDWs.

For satellite winds, horizontally filtered random instrument errors were added, as detailed below. Error magnitudes were taken from Hoffman et al. (1990). Superobservations were formed.

The CDWs simulated by Dey *et al.* (1985) have random error only, whereas we know a sizable fraction of the error is due to height assignment errors (McPherson, 1984). Further sources of error are the fact that cloud base not the cloud top may be the best level for assigning the winds and the deviations from unit emissivity for the cloud. These errors, especially the height errors tend to be very well correlated (at least at a particular synoptic time) for a particular data producer. The cause of the height assignment errors is fundamental. Generally two approaches to height assignment have been used:

1 The climatological approach. For example, assigning all low level wind to 900 hPa or assigning all high level wind to the climatological tropopause
2. IR radiance approach. In this technique the observed IR cloud radiance is used to deduce a cloud top temperature, which is then matched to a temperature profile specified from a recent analysis or short term forecast.

The CDWs simulated by Dey *et al.* essentially used an error free temperature profile for height assignment. We could reassign the pressures by adding an ad hoc error to the CDW pressures directly, or by assuming an ad hoc temperature error and reassigning the pressure by comparing the "observed" temperature to the nature run. These errors would have to be fairly large. These approaches would indirectly create horizontally correlated errors.

We have chosen to more directly induce correlated errors in the CDW data by spatially filtering the errors in the simulated data We divided the data into high and low winds and filtered the u and v wind components for each group separately. As seen in figure A.1 the distribution of observing pressures has two major modes and we choose 600 hPa as the dividing pressure The data are for 12 UTC, 21 November 1979; there were a total of 1935 CDWs. The filter we use is a weighted average followed by an amplification step. The averaging reduces the amplitudes of the original errors, while inducing correlations The amplification step multiplies all weighted average errors by a constant factor to restore the original amplitude of the error variance. This constant is equal to the variance of the original errors divided by the variance of the filtered errors The weighted average operator is equivalent to the first pass of a

Barnes filter (Koch *et al.*, 1983) The weights, w, are given by in terms of the distances, d, between the point to be filtered and the nearby points, according to

$$w = \exp\left(-\left(\frac{d}{d_0}\right)^2\right) \tag{A1}$$

Here d_0 is the scale of the filter and all points within $2 \times d_0$ are included in the weighted average. After filtering a random error field, correlations drop to approximately 0.5 at a separation distance of *do*. We chose d_0 to be 0.1 earth radii or approximately 637 km

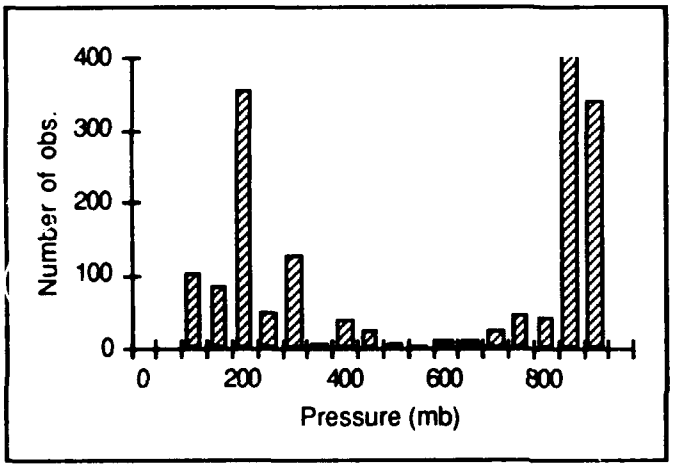

Fig. A.1. Distribution of CDW pressures.

The results of the filter on the horizontal correlations of the CDW errors is shown in figures A.2and A.3 for the low and high wind groups. For reference the correlation of the nature run evaluated at the same data locations is presented in the upper row of plots. Correlations of the original errors are displayed in the center row and correlations of the filtered errors are displayed in the lower row of plots. As indicated the results for the u and v wind components are displayed in the left and right columns respectively. Note that the errors are treated by the filter as if they were all at a single level (separately for high and low winds). On the other hand, the nature data used for the correlations are at a variety of pressure levels. The synoptic scale is clearly evident in the v correlations from the nature run. This is not obvious in the u correlations because of the strong zonal component, especially at higher levels.

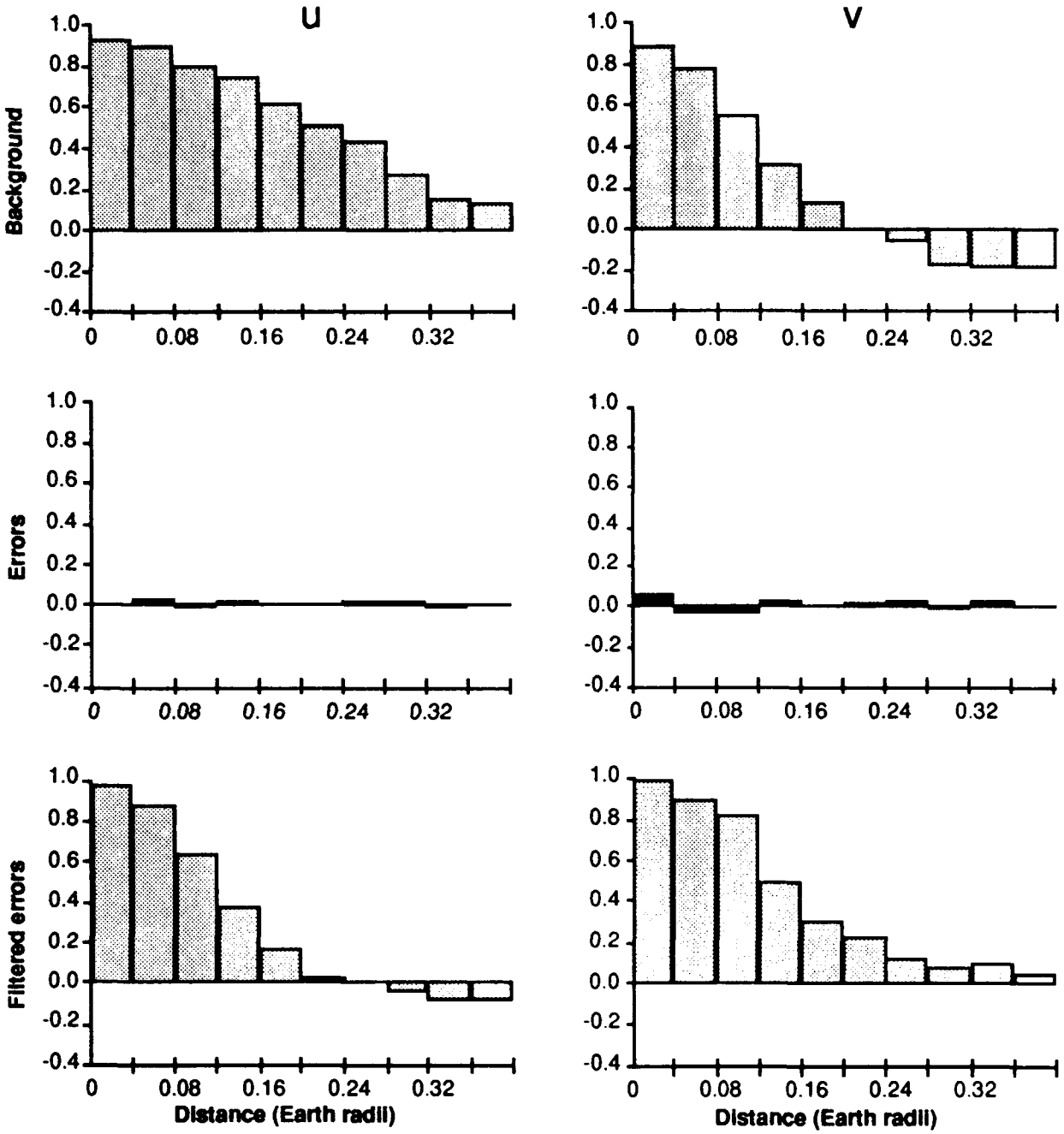

Figure A.2: Horizontal correlations for low level (1000-600 hPa) CDWs. Shown are correlations for the background field evaluated at the CDW locations (top), original CDW errors (middle) and filtered CDW errors (bottom) for u (left) and v (right) wind components.

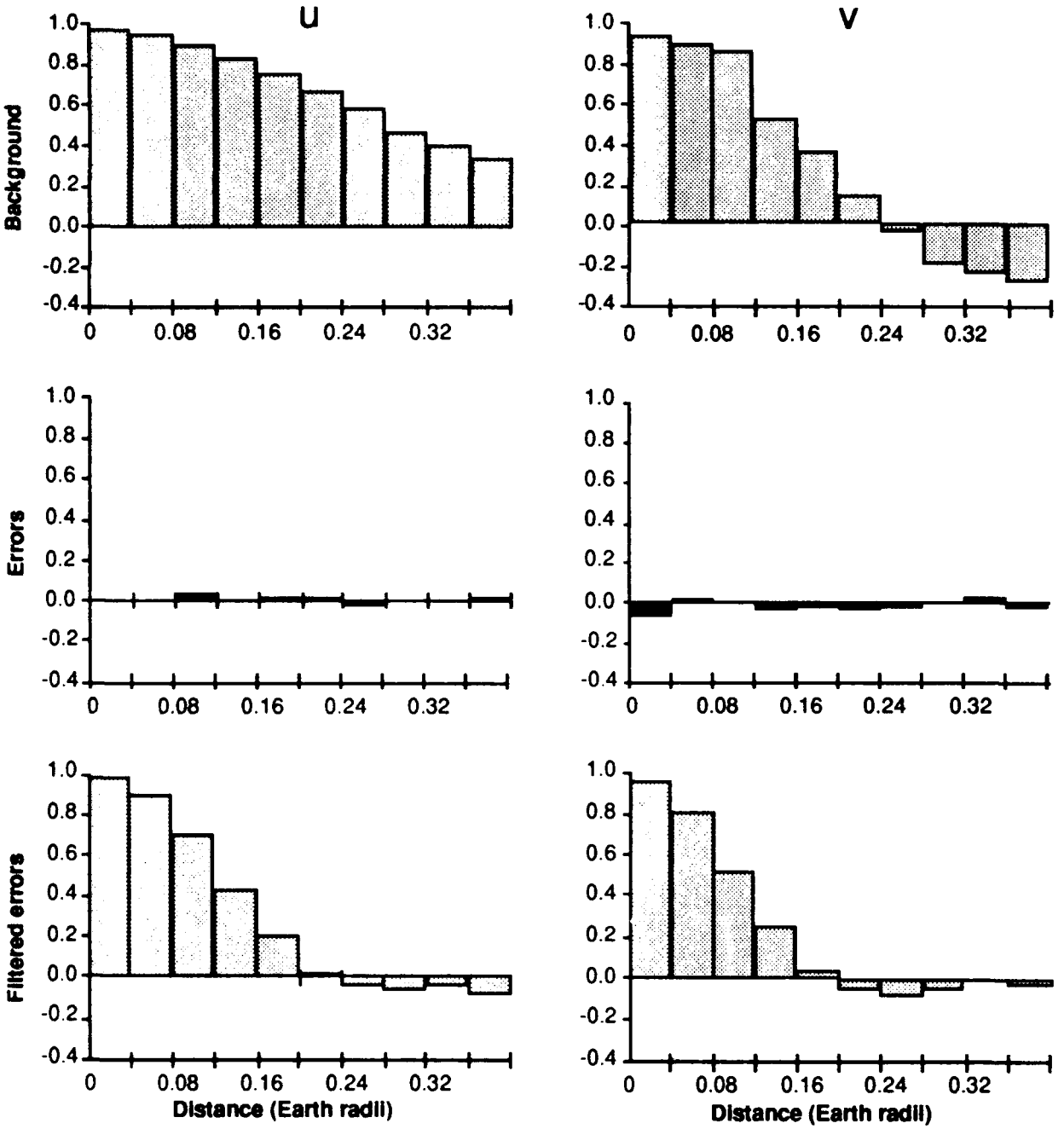

Figure A.3: Horizontal correlations for high level (600-100 hPa) CDWs. Same as Fig. A.2.

Appendix B: Simulation of optimal radiance retrieval using SSM/T data

B.1 Methodology

The radiance retrieval is a step in CASCADE following the OI, but preceding the OI postprocessor (OIPTS). As implemented in our OSSEs, gridded output from the OI was used as the first guess for the retrieval, and updated values were used at grid points with SSM/T data. The horizontal interpolation from analysis grid points to sounding locations (and vice versa) was not explicitly simulated. To eliminate difficulties with variable surface emissivities which occur over land or ice, retrievals were computed only at grid points over water, and equatorward of 65°. Satellite track computations were used to determine the data swaths for each 6-hour interval, and only gridpoint within those swaths were used in the retrievals. Out of the total of 6642 analysis grid points over the globe, 1782 (27%) are poleward of 65°, and 1402 (21%) of the remainder are over land. For 06 UTC analysis time periods, 2269 (34%) of the remaining points were not covered by the DMSP satellite, and 1189 (18%) were used in the retrievals. Similar distributions of points apply to the other analysis time periods.

B.1.1 Retrieval method

The formulation of the simulated errors is based on Eyre (1988) and Eyre (1989) analysis, as follows.

Linear optimal retrieval, like many other retrievals, may be written as:

$$\hat{x} - x_o = \mathbf{W}\left(y_m - y_c(x_o)\right), \tag{B1}$$

where $\hat{x}$ = retrieval
x_o = first guess
$\mathbf{W}$ = weight matrix
y_m = measured radiances
y_c = calculated radiances

Nonlinear optimal retrieval involves an iteration

$$x_n = x_{n-1} + \mathbf{W}\left(y_m - y_c(x_{n-1})\right) + \mathbf{B}(x_o - x_{n-1}) \tag{B2}$$

where **B** is a matrix controlling how much and in what way the retrieval may deviate from the first guess.

At convergence ($x_n = x_{n-1} = \hat{x}$), so that

$$\hat{x} - x_o = \mathbf{B}^{-1}\mathbf{W}\left(y_m - y_c(\hat{x})\right) \tag{B3}$$

In both cases we have

$$\hat{x} - x_o = \mathbf{B}^{-1}\mathbf{W}\left(y_m - y_c(x_b)\right) \tag{B4}$$

where x_b is x_o in the linear case and $\hat{x}$ in the nonlinear case and $B=I$ for the linear case. For our error analysis we linearize ym. First

$$y_m = y_c(x_T) + \varepsilon_f + \varepsilon_i \tag{B5}$$

where x_T = true state vector
ε_f = forward problem errors including factors left out of x
ε_i = instrument errors

Then,

$$y_c(x_T) = y_c(x_b) + \mathbf{K}(x_T - x_b) + \varepsilon_\ell \tag{B6}$$

where $\mathbf{K}$ = derivative of forward problem with respect to x, evaluated at x_b
ε_ℓ = linearization error

Combining the last 3 equations:

$$\hat{x} - x_T = x_o - x_T + \mathbf{B}^{-1}\mathbf{W}\left(\mathbf{K}(x_T - x_b) + \varepsilon_m\right) \tag{B7}$$

where $\varepsilon_m = \varepsilon_f + \varepsilon_i + \varepsilon_\ell$

So far we have made no approximations; modeling ε_m will require several. In the linear case, $x_b = x_o$, $\mathbf{B} = \mathbf{I}$ and

$$\hat{x} - x_T = (\mathbf{I} - \mathbf{WK})(x_o - x_T) + \mathbf{W}\varepsilon_m \tag{B8}$$

For the linear optimal retrieval

$$\mathbf{W} = \left(\mathbf{C}^{-1} + \mathbf{K}^T\mathbf{E}^{-1}\mathbf{K}\right)^{-1}\mathbf{K}^T\mathbf{E}^{-1} = \mathbf{C}\mathbf{K}^T\left(\mathbf{K}\mathbf{C}\mathbf{K}^T + \mathbf{E}\right)^{-1} \tag{B9}$$

Here **E** is the covariance matrix of the measurement and forward model errors, **C** is the covariance matrix of the background errors, and **K** is the matrix of the derivatives of y with respect to x, that is the derivative of the forward problem.

In the nonlinear case, $x_b = \hat{x}$ and

$$\left(\mathbf{I}+\mathbf{B}^{-1}\mathbf{W}\mathbf{K}\right)\left(\hat{x}-x_T\right)=\left(x_o-x_T\right)+\mathbf{B}^{-1}\mathbf{W}\varepsilon_m \tag{B10}$$

For the optimal retrieval

$$\mathbf{W}=\left(\mathbf{K}^T\mathbf{E}^{-1}\mathbf{K}+\mathbf{C}^{-1}\right)^{-1}\mathbf{K}^T\mathbf{E} \tag{B11}$$

$$\mathbf{B}=\left(\mathbf{K}^T\mathbf{E}^{-1}\mathbf{K}+\mathbf{C}^{-1}\right)^{-1}\mathbf{C}^{-1} \tag{B12}$$

Therefore

$$\left(\hat{x}-x_T\right)=\mathbf{B}\left(x_o-x_T\right)+\mathbf{W}\varepsilon_m \tag{B13}$$

This is very much like the original nonlinear iteration of Eq. (B2).

To apply these relationships, in general we need **W**, **K** and **B** as well as x_0 and x_T and a way to model the errors. For optimal retrievals we can generate **W**, **K** and **B** from **K**, **E** and **C** used in the retrieval. In such a case the same **K** is used in the retrieval and error analysis. This is permissible so long as it is accounted for in generating that part of the error due to the linearization.

The definition of x_T is troublesome. In many OSSE setups x_T does not contain enough small scales. An increment should be added to the nature run to account for scales between the scales observed by the instrument (the volume of the atmosphere it averages over for space based instruments) and the scales represented in the nature run. It is probably safe to consider these increments independent and uncorrelated from each other.

Generating the errors is simple if they can be modeled as normally distributed random variables with a known bias and channel-channel covariance matrix and no correlations in the horizontal direction. These statistics might even be stratified by location, surface type, etc. For example, suppose e is the error, b its bias and **E** its covariance matrix. Then let **A** be the matrix of eigenvectors of **E** and **D** the diagonal matrix of the square root of the eigenvalues of **E** (i.e. $\mathbf{E}=\mathbf{ADDA}^T$). The modeled error is then given by $b+\mathbf{AD}u$, where u is normally distributed with zero mean and unit variance.

Of course the errors are horizontally correlated. Even if the instrument error is not, the forward problem and linearization errors are. If these horizontal correlations are small compared to that of the first guess error (x_0-x_T) it is fair to ignore them. To assess this we may compare estimates of both correlations. The magnitude of the first guess error correlations are fairly well known from previous studies for OI schemes. The forward problem errors might be studied in simulation using a more accurate radiative transfer model.

B.1.2 Pre- and postprocessing

The forward problem for the computation of the radiances uses a perfect input profile (bilinearly interpolated from 1° by 1° nature data) at the nature run mandatory pressure levels, with errors of representativity added for a 125 km averaging length scale. The standard deviations of these errors are 0.7 K for temperature, and 1.3 m/s for wind components, and 0.1 for relative humidity. The values for temperature and winds are based on Nastorm and Gage. The value for humidity is *ad hoc*. Appropriate instrument errors were added to the radiances computed from the forward problem.

The background for the retrieval is obtained from the analysis. The output from the OI consists of analysis values of temperature T and specific humidity q, along with estimates of the analysis error standard deviations of geopotential height z and relative humidity rh, all on sigma layers. The Eyre retrieval, on the other hand, requires background values, and the complete error covariance matrix of T and log (q) on 40 (15 for moisture) pressure levels extending to 0.1 hPa. Thus, a certain amount of pre- and postprocessing was required.

As a first step, the analysis values were used to compute an updated surface pressure, and sigma layer pressures were derived from the result. The analysis values of T and q (converted to log(q)) were inter/extrapolated to the mandatory pressure levels (constant values were used for extrapolation), along with the estimated analysis errors of rh. Interpolated values of moisture were checked for supersaturation.

The estimated analysis errors of height (on σ layers) were converted to those of temperature by first constructing a height error covariance matrix, using the following specified error correlation structure:

$$r_{kl} = \frac{1}{1 + V_{ko}(\ln \frac{P_k}{P_l})^2} \qquad \text{(B14)}$$

with V_{ko}=1.098. The value of the constant was obtained by fitting this curve to the RAOB error correlation values used in the simulation of RAOB data. The covariances of height are then related to those of temperature through (Eyre, 1989):

$$\mathbf{S}_T = \mathbf{H} \cdot \mathbf{S}_z \cdot \mathbf{H}^T, \qquad \text{(B15)}$$

where $\mathbf{H} = \mathbf{L}^{-1}$, L being the operator that relates T to z ($z = \mathbf{L}.T$), and $\mathbf{S}_T$, $\mathbf{S}_z$ are the error covariance matrices of heights (z) and temperature (T). The above relationship follows directly from the definition of $\mathbf{S}_T$ and $\mathbf{S}_z$:

$$\mathbf{S}_z = \langle z \cdot z^T \rangle, \tag{B16}$$

$$\mathbf{S}_T = \langle T \cdot T^T \rangle = \langle (\mathbf{H} \cdot z) \cdot (\mathbf{H} \cdot z)^T \rangle = \mathbf{H} \cdot \langle z z^T \rangle \mathbf{H}^T, \tag{B17}$$

where < > denotes the expectation operator.

The above calculation was only done for a subset of the σ layers (the bottom-most and top-most layers were excluded), because otherwise an ill-conditioned matrix resulted in unreasonably large temperature errors (20 - 30 K). Using only the central σ layers more reasonable values for the temperature errors (1 - 5 K) were obtained. Temperature errors were further constrained explicitly to the interval 0 to 4K. Temperature errors for the bottom and top layers were set equal to the next computed layer. We removed the barotropic error variance from the height errors before this calculation, assuming it was equal to the height error at the bottom-most σ layer. The resulting temperature error standard deviations were then interpolated to the mandatory pressure levels, along with the estimated analysis errors of *rh*, but no extrapolation is done at the top. Analysis errors of *rh* were then converted to those of log(*q*) following Eyre (1989, App. B):

$$\ln q = \ln q_s + \ln rh \tag{B18},$$

which implies

$$d \ln q = d \ln q_s + d \ln rh = c_1 dT + \frac{drh}{c^2}, \tag{B19}$$

with $c_1 = \frac{d \ln q_s}{dT} \cong .08\ \mathrm{K}^{-1}$, and $c_2 = rh \cong .7$, so that

$$\langle \ln^2 q \rangle = \frac{\langle rh^2 \rangle}{c_2^2} + 2\frac{c_1}{c_2} \langle rh\, T \rangle + c_1^2 \langle T^2 \rangle, \tag{B20}$$

and

$$\langle rh^2 \rangle = c_2^2 \left[\langle \ln q^2 \rangle - 2\, c_1 \langle \ln q \cdot T \rangle + c_1^2 \langle T^2 \rangle \right]. \tag{B21}$$

We used equation(B20), with the additional assumption that $\langle rh \cdot T \rangle = 0$, to convert $\langle rh^2 \rangle$ into $\langle \ln^2 q \rangle$, and (B21) for the reverse computation.

All mandatory pressure level data were then inter/extrapolated to the retrieval pressure levels (using the same matrices as in the simulation of the statistical retrievals of TOVS data). Using specified error correlation structures (from ECMWF first guess error statistics), the retrieval level error covariance matrix was then constructed, and the Eyre retrieval computed.

The output of the Eyre retrieval was then interpolated back to sigma layers as follows: the temperature error covariance matrix, and the error standard deviation of *rh* (all at retrieval pressure levels) were extracted from the updated error covariance matrix. The temperature error covariances (on retrieval p levels) were then converted to height errors (using $\mathbf{S}_z = \mathbf{L} \cdot \mathbf{S}_T \cdot \mathbf{L}$), and all pressure level values interpolated back to sigma layers. Sigma layer values of temperature and q were updated by the interpolated increment of temperature and log(q), estimated analysis errors were replaced by their interpolated values (if they were smaller than the input; in the case of height, the barotropic component was added back in). All retrieved and interpolated values were checked for supersaturation.

B.2 Retrieval results

Before implementation of the radiance retrieval in the OSSE, some off-line tests were conducted using the analysis from the CONTROL OSSE for 00 UTC 24 Jan. as the background field. These tests all were based on comparisons of data at mandatory pressure levels before and after the retrieval steps.

Examination of individual profiles showed retrieved values closer to nature than the first guess at most levels, while some levels showed increments in the wrong direction, and some in the right direction, but overshooting. It was verified that all the interpolations are correct, and the output errors of z and *rh* are properly decreased. In general, the actual temperature errors of the first guess are smaller (order 1-2 K in the troposphere) than the error estimates (most likely an artifact of the height to temperature conversion), but they nevertheless show the correct dependence on the estimated height analysis errors, and the output height errors are properly decreased due to the retrievals (the same holds for the *rh* errors).

Using zero instrument and representativity errors, retrieval increments of temperature were generally small in the troposphere (rms decrease of error compared to first guess of order .1 K or less). At the tropopause (150 hPa), and at 300 and 250 hPa there was a slight degradation (less than .2 K). Relative humidity error showed a uniform reduction due to the retrievals.

Adding instrument and representativity errors degrades the retrievals slightly, to the point where there is negligible positive impact or a slight degradation in the troposphere. In the stratosphere there is a positive impact (.08 K to 1.27 K between 100 hPa and 50 hPa, 3.63 K at 30hPa).

Mandatory level error statistics were also collected during the radiance retrieval step during the SSMTRAD OSSE. Fig. B.1 shows the difference in mean and rms errors of the analysis grid point values before and after the radiance retrieval from the whole seven day assimilation, computed only for those points at which retrievals were performed. In general terms, these results agreed with our previous off-line calculations.

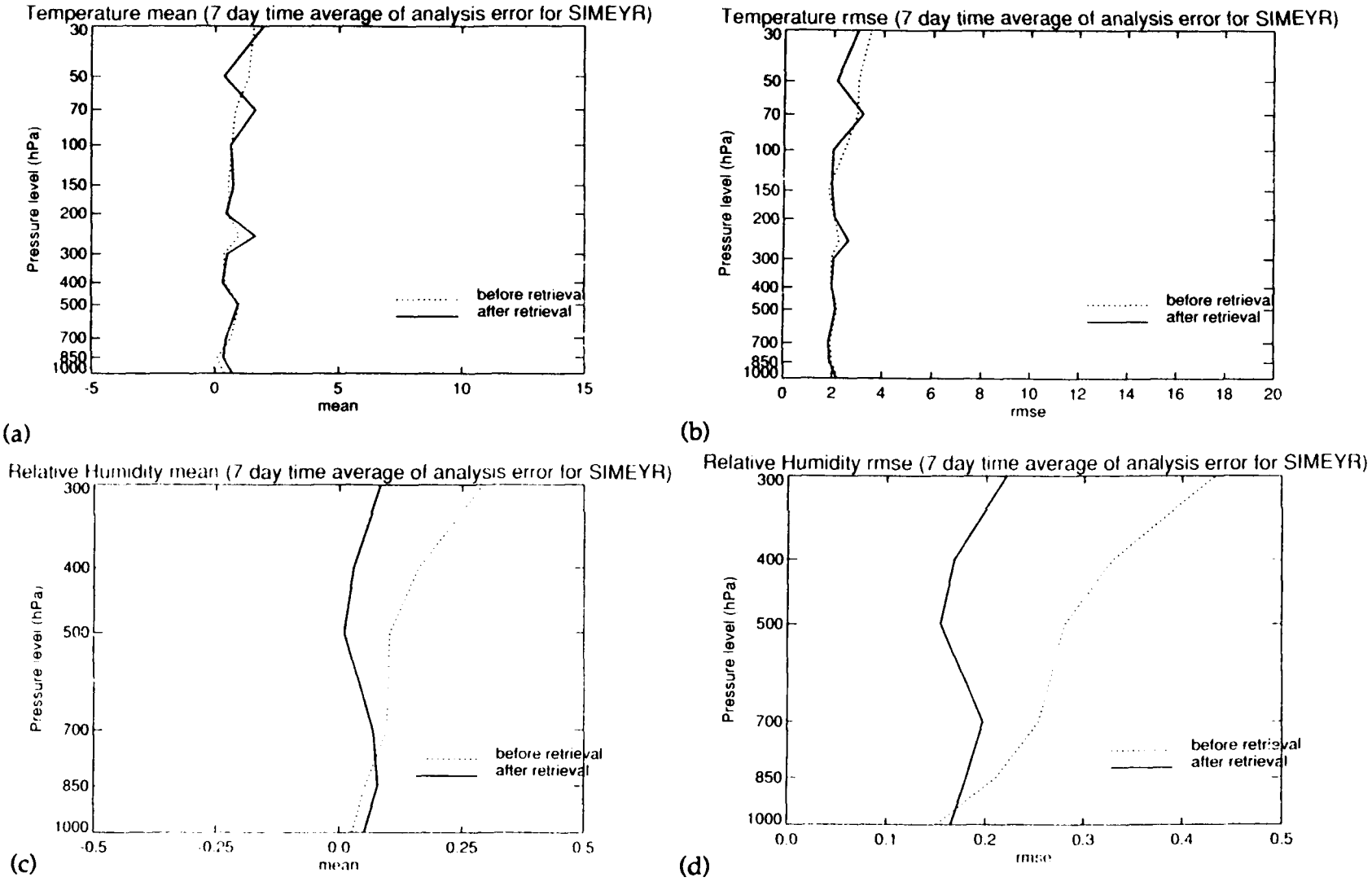

Fig. B.1: Mean (a, c) and rms (b, d) errors of temperature (a, b) and relative humidity (c, d) before and after the retrieval (dotted and solid lines, respectively). Statistics are from the 7-day assimilation for all analysis grid points for which retrievals were computed.

Errors of relative humidity show a uniform improvement between 850 hPa and 300 hPa, with reductions up to 20 %. At 1000 hPa, there is a slight degradation. The *rh* error reductions are due to both a reduction in the bias and standard deviation.

Temperature errors show almost no impact in the troposphere, except that a warm bias is introduced by the retrieval at 250 hPa. In the stratosphere, there is a reduction of error (on the order of 0.5 K), except at 70 hPa the retrieval also introduces a warm bias, which leads to an overall degradation at that level. At the topmost mandatory level (10 hPa, not shown) the analysis errors before the retrieval are quite large (16 K), and the retrieval impact is on the order of 10 K. However, since the topmost σ layer is at approximately 20 hPa, the analysis errors are due largely to extrapolation errors, and the retrieval impact is largely lost in the interpolation from pressure back to σ layers.

The small impact of the retrieval on temperature errors in the troposphere is consistent with the error characteristics of the instrument and the small first guess errors. However, the degradation at 250 hPa and 70 hPa is somewhat puzzling. One possible explanation is that the error covariance matrix used in the retrieval was incorrect, a distinct possibility since it was derived through a number of steps with several ad hoc assumptions about underlying error characteristics. Another possibility is that because the problem is so severely underdetermined (only 11 channels were used in the retrieval of 40 temperature and 15 moisture values) the matrix inversions were ill-conditioned.

Appendix C: Moist Initialization

The moist initialization was designed to explore and test methods of using observed precipitation rates in the CASCADE data assimilation scheme. In this exploratory study, no errors were added to the nature run precipitation. The impacts thus represent an upper limit for the techniques employed here. The methods were implemented as an initialization step and a forecast modification of the first guess forecast. The forecast modification consisted of a rescaling of the predicted convective heating (and precipitation) by the ratio of observed to predicted convective precipitation for all grid points in the tropics with non zero predicted convective rain. The factor was not allowed to exceed the maximum value of 10. The initialization step followed all other analysis/retrieval steps of CASCADE. In the MOIST INIT OSSE, it was inserted after the OI and before the next 6-hour forecast; in the CASCADE OSSE, it followed the SSM/T radiance retrieval step. The three components of the initialization step consisted of a diabatic NMI, a separate divergence adjustment step in which vertical profiles of horizontal divergence were adjusted based on observed precipitation rates, and a temperature and moisture adjustment step designed to bring predicted convective precipitation rates in closer agreement with observations. In the following, we describe the three components and their combination into one initialization procedure, along with test results from a case study forecast. Results of the moist initialization OSSEs are discussed in the context of the other OSSEs.

C.1 Diabatic NMI

Implementation of the diabatic NMI required only minor changes to the global spectral model (GSM). Changes were made to include physical processes in the tendency calculations, and to convert the adjustments in the moist physics (Kuo convection, large-scale precipitation, and dry adiabatic adjustment) into tendencies. In the tropics, we scaled the predicted convective heating by the ratio of observed to predicted precipitation (as in the forecast modification for the first guess forecast). This amounts to using observed column integrated latent heating rates, but only at model grid points with convection.

The same 2-iteration Machenhauer initialization scheme was used as in the adiabatic NMI in the other OSSEs, using six vertical modes and a 48 hour frequency cutoff.

C.2 Divergence adjustment

C.2.1 Determination of divergence profile

Julian (1984) has shown that the vertical profile of divergence, or, equivalently, vertical velocity, can be related to cloud top equivalent black body temperature (EBBT) in the tropics, a quantity closely related to convective precipitation rate. Kasahara et al. (1988) devised a scheme in which a parabolic vertical profile of vertical velocity was prescribed for points with EBBTs colder than a threshold value (presumed to be precipitating), and the maximum value was linearly related to the difference between observed and threshold EBBT. For cloud-free points, vertical velocity was determined as a residual from the thermodynamic equation.

We investigated several different approaches to specifying divergence in the tropics from the observed precipitation. Motivated by the approach of Kasahara, which implies a linear vertical profile of divergence for precipitating points, we computed linear regression statistics of divergence (D) or divergence divided by convective rain rate (D/R) against pressure. Nature run divergence D and D/R on either the R40 transform grid (128×102) or T106 grid (320×160) were regressed against pressure for points with $R>\varepsilon$, where ε is a specified lower limit. The convective rain rate from the nature data was computed as a 6-hour average centered around the analysis/initialization time, and interpolated horizontally as necessary. Results from a test of this method (using data from 12 UTC January 20) revealed several shortcomings, which were not appreciably different for the R40 and T106 grids. Most importantly, there was a large amount of scatter, particularly if ε was chosen small enough so that a substantial number of grid points were included in the sample. Correlation coefficients were less than 0.1 if all rainy points (53% of all points) were included, and less than 0.2 if only 31% of all points were included. In addition, correlation coefficients were larger (although only slightly) for D than for D/R, indicating a fundamental problem of relating the strength of the ascent to the intensity of precipitation in the straightforward manner attempted here. This is due to the fact that R varies over several orders of magnitude, thus making the quantity D/R a highly variable quantity.

To avoid the problems encountered in the linear regression techniques, we computed mean profiles of vertical velocity and divergence for several categories of grid points in the tropics, each category being defined by upper and lower limits of observed convective precipitation rates. This was done for both the R40 and T106 grids, and for D and vertical velocity on pressure levels and D on σ layers (from a preprocessed version of the nature run data), and using both convective and total precipitation. An example of the results is shown in Figure C.1, which shows the mean profiles of D (along σ surfaces) for 5 categories on the R40 transform grid. The definition of the categories in terms of total rain rate is given below. Only grid points equatorward of 30° were used in the statistics.

Table C.1: Definition of categories 1 - 5. R_{low} and R_{upp} are the lower and upper limits of rain rate (note that 10^{-8} m/s corresponds to 0.864 mm/day).

Category	R_{low} (10^{-8}m/s)	R_{upp} (10^{-8}m/s)	Number of grid points	Percentage of grid points
1	-	1	17669	68%
2	1	5	4026	15%
3	5	10	1691	6%
4	10	50	2496	10%
5	50	-	230	1%

The profiles shown in Fig. C.1, which were based on 3 days of nature run data (12 UTC 20 January through 00 UTC 23 January) show a clear connection between rain rate and low level (upper level) convergence (divergence). There is still a substantial amount of scatter: all the mean profiles except for category 5 are within one standard deviation of one another; however, the mean profiles from the aggregate statistics of the 3 days (6 time periods) shown in Fig. C.1 agree well with those computed for individual time periods.

We tested the sensitivity of the results to a number of factors, but all showed a negligible effect. The results shown in Figure C.1 are virtually identical when convective rather than total rain rate is used. Profiles for divergence along pressure surfaces (rather than σ) are also very similar, except that the differences between the category means are slightly larger; however, standard deviations at low levels are also larger. Profiles of vertical velocity are consistent with those of divergence, showing ascent (descent) for rainy (dry) categories. Results are virtually identical for the R40 and T106 grids.

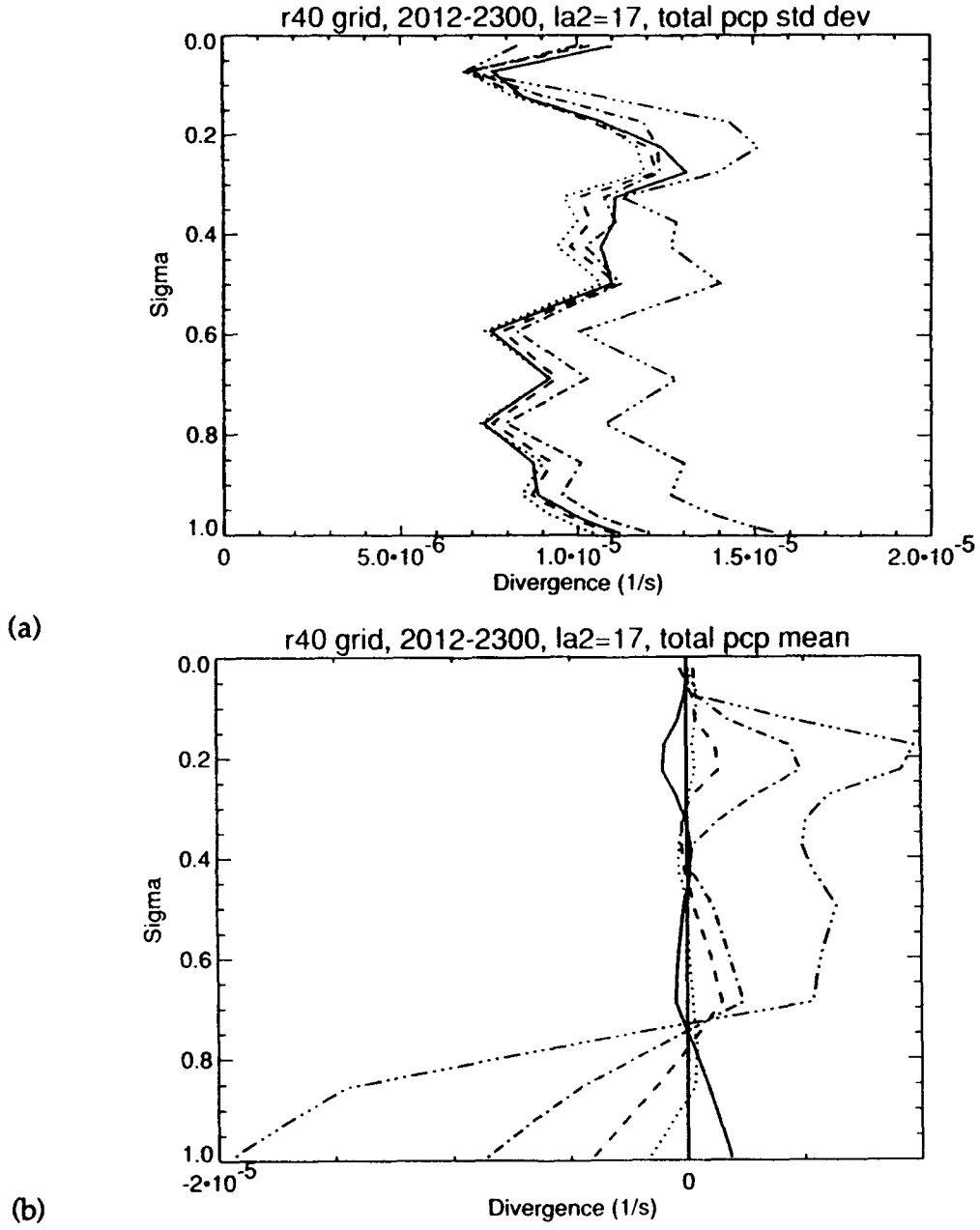

Fig C.1: Profiles of divergence along σ surfaces for 5 different categories of rainfall rate for grid points in the tropics. Category 1 is shown in solid, 2 in dotted, 3 in dashed, 4 in dash-dotted, and 5 in dash-dot-dot-dot.

C.2.2 Adjustment procedure

Based on the tests described above, the following divergence adjustment procedure was implemented. For each gridpoint equatorward of 30°, the category (1-5) was determined from the observed total rain rate. The analysis divergence profile was then replaced by the divergence profile corresponding to the rainfall category, with the following modification: (1) to avoid unreasonably sharp gradients at the boundary of the adjusted region, analysis

and specified divergence profiles were combined as a weighted average at the latitude circles at the boundary; (2) to avoid changing the vertical average of divergence, the vertically averaged difference between analysis and specified divergence is added to the specified divergence profile. Thus, if we denote the original divergence by d and the divergence profile of category i by c^i, and their respective vertical integrals by D and C^i, then the modified divergence after the first step of the adjustment (d^1) for a grid point with category i is given by:

$$d^1 = (1-w)\, d + w\, (c^i + D - C^i)\,, \tag{C1}$$

where w is the blending weight (w=1 for all latitudes equatorward of 30°, and w=0.5 for the latitude circle poleward of 30°). The blending of analysis and specified divergence fields at the edge of the tropics is similar to the procedure employed by Kasahara et al. (1988). To avoid changes to the divergence field outside the tropics, a technique similar to one employed by Kasahara et al. (1988) was implemented here. Rain-free grid points (category 1 in our case) were further modified in a second step by subtracting, at each level, the horizontal integral of the changes of divergence introduced in the first step, normalized by the area of category 1:

$$d^2 = d^1 - \delta_{i1} w \frac{\int w(d^1 - d)\, dA}{\int \delta_{i1} w\, dA} \tag{C2}$$

Here δ_{i1} is the Kronecker delta (=1 for points with category 1, =0 otherwise), and the area integral extends over all grid points with non zero w. This ensures that the horizontal integral of divergence in the tropics is unaffected by the divergence adjustment.

C.3 Temperature and moisture adjustment

In contrast to the empirically based divergence adjustment, adjustment of moisture and temperature values in order to achieve better agreement of predicted and observed convective precipitation is quite model-dependent. With the present version of the model, which uses the Kuo convection scheme, we could draw upon the experience of Donner and Rasch (1989) and Krishnamurti et al. (1984). In Donner and Rasch, the initial state values of moisture are adjusted to obtain the desired precipitation, and temperature values are adjusted to obtain the desired heating rate. The adjustments are performed as part of a variational scheme under the additional constraint of minimizing the column integrated squared adjustments. Because derivatives of precipitation and heating with respect to the input profiles of temperature and moisture are discontinuous across the point of conditional instability, low-level values of temperature and moisture have to be adjusted separately to ensure the presence of convection, and these values are not included in the

variational adjustment process. However, even then there will be some points for which the criteria for convection will not be satisfied, particularly if there is no or insufficient convergence of water vapor. It was found in Kasahara et al. (1992) that the separate divergence adjustment step was necessary to improve the results of the temperature and moisture adjustment.

Krishnamurti et al. (1984) use a somewhat different approach. In their work they use a "reverse Kuo", in which the preliminary predicted (not the initial values) of moisture are adjusted by a factor constant with height ($1+\varepsilon$). The adjustment step is quite straightforward in this case, since the amount of moisture convergence can be directly prescribed by the proper choice of ε. However, their approach requires a forward-backward integration during an extended pre-integration period that is as long as 2 days.

We used a combination of the two approaches in our scheme. As in Donner and Rasch, the initial state, rather than the preliminary predicted values of temperature and moisture were considered for adjustment. To include as many points as possible in the adjustment procedure, restrictions on convection (minimum values for moisture convergence) were removed, and surface values of moisture and temperature were increased at grid points which were stable but had non zero observed precipitation. Both the lowest level temperature and specific humidity were increased by a predetermined increment until a convective cloud deep enough for the production of precipitation was diagnosed, or the maximum number of iterations was exceeded.

We also attempted a simplified version of the moisture adjustment, in which the initial moisture values above the surface were modified by a factor ($1+\varepsilon$), similar to Krishnamurti's approach. A closed-form solution for this factor was derived from an approximation of the modified convective precipitation resulting from this adjustment. This derivation is reproduced in the following:

In the version of the Kuo scheme implemented in our GSM, the convective precipitation rate, R, is given by (neglecting the reevaporation of falling precipitation)

$$R = \frac{P_s}{g} \cdot w \cdot (1 - b) \ , \qquad \text{(C3)}$$

where P_s is the surface pressure, g the acceleration of gravity, w the moisture convergence, and (1-b) the heating/moistening partitioning parameter. The moisture convergence is given by the vertical integral

$$w = \int_{\sigma_t}^{\sigma=1} \frac{dq}{dt}\, d\sigma = \sum_{k=K}^{k=1} \left(\frac{dq}{dt}\right)_k \Delta\sigma_k \ , \tag{C4}$$

where σ_t, k_t denote the cloud top, and $\left(\frac{dq}{dt}\right)_k$ is given by

$$\left(\frac{dq}{dt}\right)_k = \begin{cases} (q_k^{t+1} - q_k^{t-1})/(2\Delta t) & \text{for } t \geq 2 \\ (q_k^{t+1} - q_k^{t})/\Delta t & \text{for } t = 1, \end{cases} \tag{C5}$$

since a forward step is used for the first time step, and leap-frog steps thereafter. Finally, the parameter b in this scheme is computed from

$$b = \frac{\int \omega \left[\frac{T}{\theta}\frac{c_p}{L}\frac{\partial\theta}{\partial p} + \frac{\partial q}{\partial p}\right] dp}{2\int \omega \frac{\partial q}{\partial p} dp} \ , \tag{C6}$$

with ω approximated as $\omega \equiv \tau = -\int_o^\sigma \nabla \cdot \mathbf{V}\, d\sigma$, and the vertical integrals approximated by

$$b \cong \frac{\sum \tau_k \left[\left(\frac{T}{\theta}\right)_k \frac{c_p}{L}(\theta_{k+1} - \theta_k) + (q_{k+1} - q_k)\right]}{2\sum \tau_k (q_{k+1} - q_k)} \tag{C7}$$

The sums are evaluated from cloud bottom to cloud top.

To assess the effects of modifying the initial moisture on the rain rate, we need to consider the effects on w and 1-b separately. The moisture convergence rate may be written as

$$w = \int_{\sigma_t}^{1} \frac{\partial q}{\partial t}\, d\sigma = \int_{\sigma_t}^{1} -\nabla(\mathbf{V}q)\, d\sigma - [\dot{\sigma} q]_{\sigma_t}^{1} + \int_{\sigma_t}^{1} T(\sigma)\, d\sigma + \int_{\sigma_t}^{1} q\left(C + \frac{\partial \ln p_s}{\partial t}\right) d\sigma, \tag{C8}$$

where the conservation equation for moisture was used to substitute for $\frac{\partial q}{\partial t}$, $T(\sigma)$ is the turbulent tendency, and $C = \mathbf{V} \cdot \nabla \ln p_s$. If we now consider a modified moisture,

$$q^m = (1 + \varepsilon)\, q \tag{C9}$$

the resulting modified moisture convergence is given by

$$w^m = (1+\varepsilon)\int_{\sigma_t}^{1} q(-\nabla\cdot\mathbf{V})\,d\sigma - \int_{\sigma_t}^{1} \mathbf{V}\cdot\nabla((1+e)q)$$
$$+(1+\varepsilon)[\dot{\sigma}q]_{\sigma_t}^{1} + \int_{\sigma_t}^{1}[T(\sigma^m) - T(\sigma)]\,d\sigma + (1+\varepsilon)\int_{\sigma_t}^{1} q[C + \frac{\partial}{\partial t}\ln p_s]d\sigma. \qquad \text{(C10)}$$

If we express the turbulent tendency as a flux divergence, the vertical integral reduces to the difference between the turbulent flux at cloud top and the evaporation at the surface. We may safely neglect the flux at the top, and, since the lowest level moisture will not be modified according to (C9), the turbulent contribution to $w^m - w$ can be neglected. The vertical advection term can also be neglected, since $\dot{\sigma} = 0$ at $\sigma = 1$, and $\dot{\sigma}q$ is small at $\sigma = \sigma_t$. Further neglecting $\nabla(\varepsilon\, q)$ leaves the approximate relationship

$$\delta_w = w^m - w = \varepsilon \cdot a_w$$

$$\text{with } a_w = \int_{\sigma_t}^{1} q(-\nabla\cdot\mathbf{V})\,d\sigma + \int_{\sigma_t}^{1} q[C + \frac{\partial}{\partial t}\ln p_s]\,d\sigma, \qquad \text{(C11)}$$

which can be evaluated inside the Kuo convection subroutine.

The moistening parameter is affected indirectly by the modification of the initial moisture, because its computation is based on the (t+1) time level quantities. If we neglect effects of the modified q at time t on the values of θ^{t+1}, and approximate

$$q^{m,\,t+1} \cong (1+\varepsilon)q^{m,\,t+1}, \qquad \text{(C12)}$$

which is equivalent to assuming that

$$\frac{\partial q^m}{\partial t} \equiv (1+\varepsilon)\frac{\partial q}{\partial t} \qquad \text{(C13)}$$

the integral involving q is multiplied by the factor $(1+\varepsilon)$, which results in the approximate formula

$$\delta_{1-b} = (1-b)^m - (1-b) = [\frac{1}{2} - (1-b)]\frac{\varepsilon}{1+\varepsilon}. \qquad \text{(C14)}$$

Combining the changes to w and 1-b results in the modified rain rate

$$\delta R = R^m - R = [w\delta_{1-b} + (1-b)\delta_w + \delta_{1-b}\delta_w]\frac{P_s}{g} \qquad \text{(C15)}$$

Setting $\delta R = R^{Obs} - R$ and denoting $\delta r = \frac{g}{P_s}[R^{Obs} - R]$, results in the following equation for ε after some algebraic manipulations:

$$\varepsilon^2 \cdot c_1 + \varepsilon \cdot c_2 + c_3 = 0,$$

$$\text{with } c_1 = \frac{1}{2} a_w, \; c_2 = (1-b)\, a_w + [\frac{1}{2} - (1-b)]\, w - \delta_r, \; c_3 = -\delta r. \qquad \text{(C16)}$$

C.3 Tests of the initialization procedure

All components of the initialization procedure were tested on the last analysis from the spinup experiment (00 UTC 23 January). A number of different configurations were tested, in order to evaluate the different initialization components in isolation and in combination. The following table provides a summary of the combination of initialization steps. The primary tool for assessment was a comparison of the adjusted initial state, and of the 6-hour forecast generated from it, with the corresponding nature data.

Table C.2: Configuration of initialization experiments. Convective heating and precipitation scaled by ratio of observed to predicted precipitation during NMI and forecast in all experiments other than CONTROL. Temperature and moisture adjustment refers to the adjustment of lowest layer values only.

Name	Configuration
CONTROL	adiabatic NMI
Test A	diabatic NMI
Test B	Test A + divergence adjustment
Test C	Test B + temperature and moisture adjustment
Test D	Test A + temperature and moisture adjustment
Test E	Test C + diabatic NMI
Test F (MOIST INIT)	Test E + temperature and moisture adjustment

The diabatic NMI by itself (Test A) lead to very small differences when compared to the adiabatic NMI (CONTROL): temperature differences (vertically averaged rms differences) on the order of .09 K and wind differences of .07 m/s in the initial state, and rms differences from nature agreed to within .003 K and .001 m/s. After a 6-hr forecast, differences compared to CONTROL were still small (.1 K, .3 m/s). This result is consistent with the findings of Kasahara et al. (1992) and Knowlton et al. (1989), among others. Interestingly, forecast errors after 6 hours were worsened for temperature and winds by the diabatic NMI when compared to control, whereas the moisture errors were improved; rms errors differed by only .003 K, .02 m/s, and .01 g/kg, however.

Adding the divergence adjustment after the diabatic NMI (Test B) lead to the most noticeable changes. In the initial state, the vertically averaged rms error of the divergent wind was decreased by nearly 1 m/s (from 3.861 m/s to 2.864 m/s). The improvement due to the divergence adjustment is also reflected in the number of grid points with both observed and predicted precipitation: during the first time step of the forecast, 11.5 % of all grid points had both observed and predicted rain (hit), 40.9 % had observed but no predicted rain (miss), and 3.7 % had no observed but predicted rain (false alarm) after the divergence adjustment. The corresponding numbers for the diabatic NMI alone (Test A) were 10.4 % hits, 42.0 % misses, and 4.5 % false alarms. After a 6-hour forecast, rms errors of temperature, winds, and moisture were all decreased compared to CONTROL or the diabatic NMI alone (Test A), but the improvement in the divergent wind errors was reduced to .4 m/s. The improvement in the hit/miss statistics of observed and predicted rain did not persist past the first hour into the forecast.

The output from the divergence adjustment (Test B) was subjected to the first part of the temperature and moisture adjustment (in which only the bottom layer temperature and moisture were modified as necessary for conditional instability) in the next experiment (Test C). In the initial state, this improved the lowest level specific humidity error by .13 g/kg (from 2.76 to 2.63 g/kg); more importantly, the hit/miss statistics at the first time step of the forecast were further improved to 13.2 % hits, 39.2 % misses, and 3.8 % false alarms. As in the case of the divergence adjustments, however, the improvement in the hit/miss statistics did not persist past the first hour of the forecast. At the end of the 6-hour forecast, rms errors of temperature, winds, and specific humidity all showed improvements. Compared to CONTROL, errors were decreased by .02 K (temperature), .4 m/s (divergent wind), and .02 g/kg (specific humidity); improvements compared to the divergence adjustment forecast (Test B) were roughly an order of magnitude smaller.

The temperature and moisture adjustment of the lowest layer was also applied to the output of the diabatic NMI in Test D, to test the importance of the divergence adjustment as a first step. As might be expected from the

comparatively large effect of the divergence adjustment alone, results from this experiment were noticeably worse. The initial hit/miss statistics were 11.6 % hits, 40.8 % misses, and 4.7 % false alarms, while forecast errors were larger than in Test C for all fields, and larger than even CONTROL and Test A for temperature and winds. It is interesting to note that the temperature and moisture adjustment actually lead to a slight degradation of the temperature and wind forecast, whereas in Test C it slightly improved those errors.

The second component of the moisture adjustment, which was applied to the layers above the surface, did not achieve the desired result. It increased the initial error in specific humidity, worsened the hit/miss statistics of the first time step, and lead to increased forecast errors of specific humidity (even when compared to control). There are several possible reasons for this: one or more of the approximations made in the derivation of the equation for ε could be invalid, and there could be an error in the derivation or the coding of the scheme. Because of the limited level of effort available for this task, these questions could not be pursued further. The temperature and moisture adjustment was thus restricted to the adjustment of the lowest level temperature and moisture, which had a small, but positive impact.

Kasahara et al. (1992) experimented with several different combinations of their initialization steps, and found the following arrangement to give the best results (in terms of the precipitation spinup behavior):

step 1: diabatic NMI
step 2: divergence adjustment
step 3: temperature and moisture adjustment
step 4: diabatic NMI
step 5: temperature and moisture adjustment

We tested adding steps 4 (Test E) and 5 (Test F) to the output from our temperature and moisture adjustment and also found the best results when all 5 steps were used, although the additional improvements were quite small: compared to Test C, the initial errors were reduced by .003 K (temperature), .03 m/s (divergent winds), and .002 g/kg (specific humidity). At the end of the 6-hour forecast, rms errors were decreased by .04 m/s for the divergent wind, while other quantities showed inconsistent further improvements. Even though the additional improvements were minor, the moisture initialization used in the MOIST INIT OSSE consisted of all 5 steps listed above (Test F in Table C.2).

The characteristics of the precipitation spinup are depicted in Fig. C.2 for the various experiments. Shown are the global rate of convective precipitation, stratiform precipitation, and evaporation for each time step during the 6-hour forecast. It should be noted that the convective precipitation rate is scaled by the ratio of observed total precipitation to predicted convective precipitation

in the tropics in all experiments other than CONTROL. It is interesting to note that in our model, even in the CONTROL experiment, there is very little of the spinup seen in other models (e.g., Kasahara et al. 1992). Although both convective and stratiform precipitation undergo some transient behavior during the forecast, initial and final values after 6 hours differ by less than 30% in CONTROL. The initial convective precipitation is increased by the moist initialization, but it eventually equilibrates at a slightly lower level than in the CONTROL run. Comparison of the curves for Test C and Test F shows that the additional initialization steps reduced the amount of overshooting during the first hour.

The stratiform precipitation shows little difference between the experiments during the first hour, but a clear separation of the experiments without divergence adjustment (CONTROL, Test A, and Test D) from those with divergence adjustment (Test B, C, E, and F) in the remainder of the forecast period. Final values of the divergence adjustment group are slightly lower than CONTROL. The evaporation rate at the beginning of the forecast is slightly lowered by both the divergence adjustment and the temperature and moisture adjustment, but all experiments converge to nearly the same value at the end of 6 hours. For evaporation, the adjusted experiments exhibit more of a spinup than CONTROL. This indicates one of the weaknesses in our approach: changes in the divergence and low level temperature and moisture designed to yield better agreement between observed and predicted convection also affect evaporation, and, indirectly, the moisture convergence available for convection.

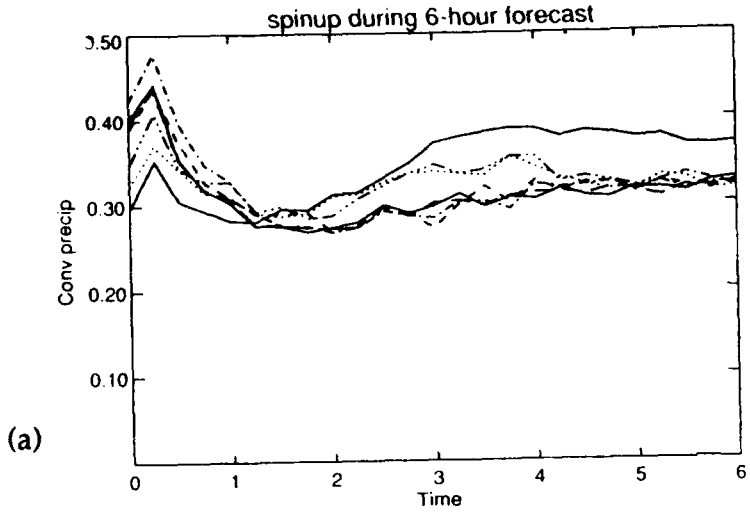

(a)

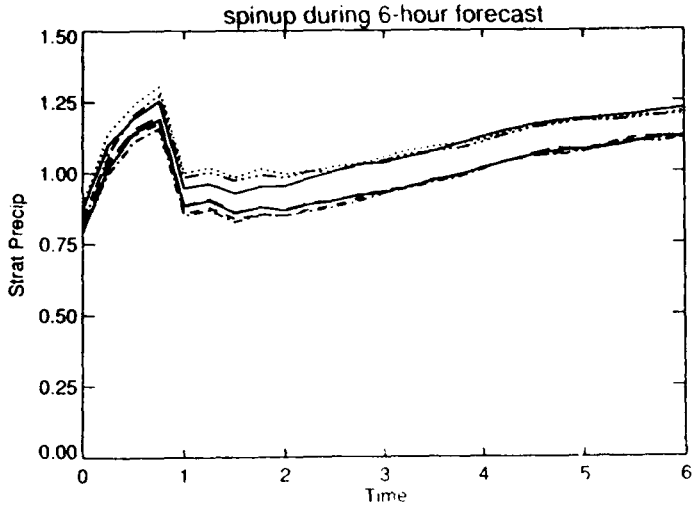

(b)

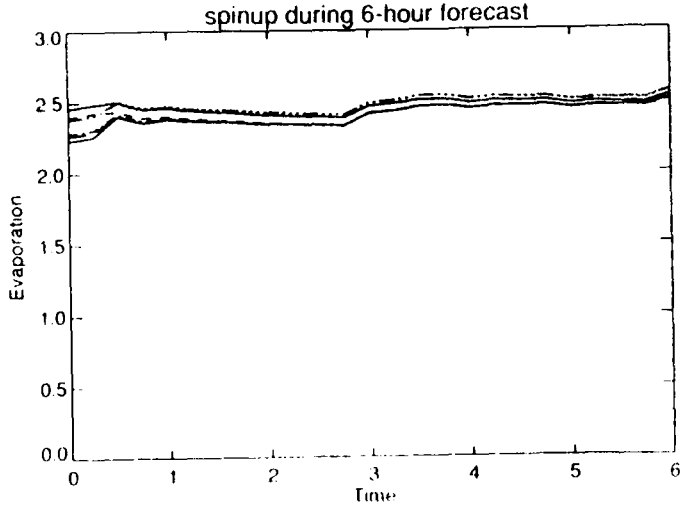

(c)

Fig. C.2: Time series of global convective precipitation (a), stratiform precipitation (b), and evaporation (c) (all in mm/day) during the 6-hour forecast of the case study. Shown are CONTROL (solid line), Test A (dotted), Test B (short dashes), Test C (dash-dotted), Test D (dash-dot-dot-dot), Test E (long dashes), and Test F (solid).